JOURNAL OF PROPULSION AND POWER
Vol. 9, No. 6, Nov.–Dec. 1993

Erosive Burning of Solid Propellants

Merrill K. King
Falls Church, Virginia 22042

Nomenclature

B = blowing parameter, Eq. (8)
b = blowing parameter, Eq. (26)
C_f = skin friction coefficient
C_h = Stanton number
D = grain port diameter
d_p = oxidizer particle diameter
G = crossflow mass flux
k_2 = erosivity constant, Eq. (2)
L_{AP}, L_I = distance from surface to AP heat release zone
L_{Diff}, FH90 = mixing distance associated with oxidizer/fuel flame
L_{fz} = fizz-zone height
L_{RX}, L_{Kin} = reaction distance associated with oxidizer/fuel flame
M = crossflow Mach number
$\dot{m}$, $\dot{m}_p$ = propellant burning mass flux
n = propellant burning rate pressure exponent
P = pressure
R_{port} = grain port radius
r = propellant burning rate
r_e = erosive component of propellant burning rate, $r - r_0$
r_0 = zero-crossflow propellant burning rate
Q_{RX} = surface/subsurface propellant heat release (per unit mass)
Q_{VAP} = heat of vaporization per unit mass of propellant
T_{AP} = AP monopropellant flame temperature
T_{dz} = double-base propellant dark zone temperature
T_f = propellant flame temperature
T_s = propellant surface temperature
u = local crossflow velocity
V = freestream crossflow velocity
x, y = distance from propellant surface
γ = specific heat ratio
ε = ratio of total burning rate to zero-crossflow burning rate, r/r_0
ε = eddy viscosity
θ = flame-bending angle, Figs. 5–7
λ = thermal conductivity
μ = laminar viscosity
ρ_{gas} = product gas density
ρ_{prop} = propellant density
τ = local shear stress

I. Introduction

A REVIEW of experimental and modeling work concerning erosive burning of solid propellants (augmentation of burning rate by flow of product gases across a burning surface) is presented. A brief introduction describes motor design problems caused by this phenomenon, particularly for low port/throat area ratio and, in the limit, nozzleless motors. Various experimental techniques for measuring crossflow sensitivity of solid propellant burning rates are described, with the conclusion that accurate simulation of the flow, including upstream flow development, in actual motors is important since the degree of erosive burning depends not only on local mean crossflow velocity and propellant nature, but also on this development. A brief review of "simplified" models and correlating equations is presented, followed by a description of more complex numerical analysis models. Both composite [ammonium perchlorate (AP)] and double-base propellant models are reviewed. A composite propellant model developed by King is shown to give good agreement with data obtained in a series of tests in which propellant composition and heterogeneity (particle size distribution) were systematically varied. Finally, use of the numerical models for development of erosive burning correlations (of particular use to the ballistician) is described, and brief discussion of scaling criteria is presented.

II. Background

The flow of combustion product gases at high velocity across a burning solid propellant surface is often found to lead to a significant increase in burning rate over that obtained at the same pressure in the absence of crossflow—this phenomenon is referred to as erosive burning and the increase in burning rate is known as the erosive burning rate. An example of this effect is shown in Fig. 1, where data of Marklund and Lake[1] are presented in the form of burning rate vs pressure curves for an AP/polyester propellant at several crossflow velocities. With most (but not all) propellants, there is a minimum crossflow velocity below which erosive burning is not observed—

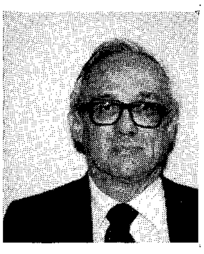

Merrill K. King received B.S., M.S., and Ph.D. degrees in Chemical Engineering from Carnegie Institute of Technology in 1960, 1962, and 1965, respectively. He is currently on assignment as Senior Visiting Scientist in the Microgravity Combustion Program at NASA Headquarters. Dr. King spent approximately two years as Program Director for the Combustion and Thermal Plasmas Program at the National Science Foundation, and a total of 26 years as Chief Combustion Scientist for the Atlantic Research Corporation. His research expertise is primarily concerned with combustion phenomena associated with various solid and liquid propellant propulsion systems. He has published numerous papers in various journals of the AIAA, in JANNAF publications, and in proceedings of the Combustion Institute. Dr. King has been quite active over the past 25 years on various AIAA and JANNAF committees and working groups. He is an Associate Fellow of the AIAA, and recently completed his fourth year as an Associate Editor for the *Journal of Propulsion and Power*.

Received Oct. 15, 1991; revision received Feb. 8, 1993; accepted for publication March 26, 1993.

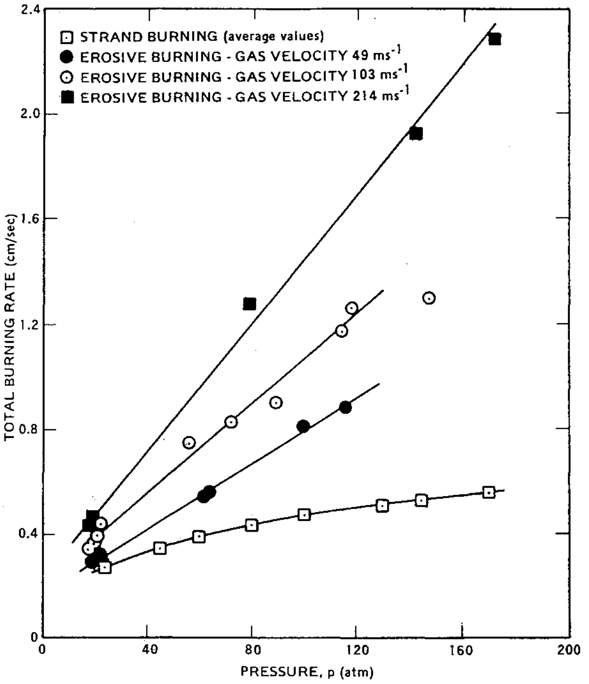

Fig. 1 Erosive burning of an AP/polyester propellant as a function of pressure at several gas velocities.[1]

this is referred to as the threshold velocity and can be as high as several hundreds of m/s, particularly for high-burning-rate formulations.

In recent years, requirements for ever higher propellant mass fractions in solid propellant rocket motors and for higher thrust-to-weight ratios have led to development of centrally perforated grain configurations with relatively low port-to-throat ratios. As a result, during the early portion of operation of such motors, there are high velocities across burning propellant surfaces in the aft portion of the grain, with these velocities rapidly decreasing with time as the grain port opens up. The erosive burning accompanying these high velocities, even though partly offset by burning rate decreases accompanying resultant pressure decrease down the bore (see Ref. 2 for sample calculations), leads to an initial overpressure relative to mean operating pressure during the early portion of the motor operation, in turn leading to the requirement for a heavier case for a given mean operating pressure (undesirable). In addition, if the designer does not somehow compensate for the unequal initial burning rates along the grain (e.g., by using a thicker web in the aft regions), the propellant will burn out unevenly, leading to a long pressure and thrust tailoff (often also undesirable).

Use of grain configurations with slots, stars, or "wagon-wheels" at various locations along the port is common practice: in many cases, velocities of gas flow in these regions can become quite high relative to mean flow through the central port, again leading to local erosive burning which must be compensated for in the motor design. Little attention has been given to this problem in published literature. A recent effort by Ayris and Petrovic[3] does address erosive burning in a star-configuration centrally perforated motor.

A series of studies has demonstrated that the nozzleless motor concept (mass flow choking at the end of a cylindrical bore) offers significant economic and operational advantages over a more conventional rocket system when considered for some tactical weapon systems (notably air-launched integral-rocket-ramjet systems, where ejection of a throat pack during transition from boost to sustain operation is highly undesirable). This concept requires that the flow within the bore or central perforation of a grain accelerate to the point that sonic conditions are achieved at the aft end. In this situation, the high velocity environment results in substantial erosive burning, with burning rates significantly higher than those measured in a conventional strand bomb being encountered.

Nozzleless rockets present a unique challenge to analytical understanding, because the gas velocity reaches sonic and supersonic velocities on the grain surfaces, leading to a realm of erosive burning never before considered. The effects are critical in that the erosive burn rate contributions strongly influence performance level, performance repeatability, and thrust misalignment. More than in any conventional motor, the exact erosive burn rate behavior must be held constant from batch to batch if reproducibility is not to be a problem. The performance sensitivity of a nozzleless motor to erosion is due to the fact that the maximum erosion occurs at the choke point in the bore. Since this point is the effective throat area, and the throat area vs time is thus a function of regression rate, the result is a chamber pressure history which varies strongly with erosion.

With nozzleless motors, the effects of erosive burning are further magnified due to higher crossflow velocities (in the Mach 1 range), and due to the fact that the aft end port/throat area ratio does not decrease with time since the aft end is the throat (in most cases). Assuming that an erosive burning rate correlation of the form $r/r_0 = 1 + k_2M$ is applicable, and allowing for the fact that static pressure decrease down the bore accompanying the velocity increase tends to decrease burning rate for propellants with a positive pressure exponent (usual), countering the erosive effects to some extent, it may be shown[2] that for a nozzleless motor with a uniform bore radius

$$r_{\text{aft}}/r_{\text{fore}} = (k_2 + 1)/(\gamma + 1)^n \tag{1}$$

where r is the local burning rate (function of pressure and crossflow velocity), γ is the product specific heat ratio, and n is the propellant burning rate-pressure exponent. Values of $(r_{\text{aft}}/r_{\text{fore}})$ as a function of k_2 and n are presented in Table 1. As may be seen, for the case of no erosion ($k_2 = 0$), the aft end will recede more slowly than the fore end, due to lower pressure at the aft end. As k_2 increases, the $r_{\text{aft}}/r_{\text{fore}}$ ratio also increases, going through unity (generally desirable) at a value of k_2 which depends on the burning rate exponent. The results of Table 1 give some indication of the sensitivity of nozzleless motor design to the erosive burning characteristics of the propellant, and therefore, further point out the importance of information regarding the propellant's erosive burning characteristics to the designer.

Since there is such a strong interaction between the local flow environment and the propellant burning rate, it is necessary to be able to predict this interaction in order to design and calculate the performance of a low port/throat area ratio rocket (particularly a nozzleless rocket with a port/throat area

Table 1 Simplified ballistic analysis of a nozzleless motor with uniform port area

$r/r_0 = 1 + k_2M, \quad r_0 = bp^n$

n	k_2	$r_{\text{aft}}/r_{\text{fore}}$
0.4	0.0	0.72
	0.5	1.08
	1.0	1.45
	1.5	1.80
0.6	0.0	0.61
	0.5	0.92
	1.0	1.23
	1.5	1.54
0.8	0.0	0.52
	0.5	0.78
	1.0	1.05
	1.5	1.31

ratio of unity). With such a predictive capability, the motor designer can either design his grains to compensate for mean erosive burning effects on grain burn pattern, or, knowing how propellant formulation parameters affect erosion sensitivity, vary propellant parameters in such a way as to minimize these effects. Accordingly, considerable effort (experimental and analytical) has been carried out over the past few decades with the goals of understanding, being able to predict, and being able to control erosive burning characteristics of solid propellants. An excellent review of much of this work is presented in Ref. 4.

III. Experimental Studies of Erosive Burning

In the experimental characterization of erosive burning of solid propellants, the investigator is faced with a conflict between a desire to perform inexpensive tests with relatively easy direct measurement of burning rate in the presence of crossflow (as exemplified by tests in which a hot product gas is passed over strips or pellets of the propellant of interest, with relatively easy optical access for measurement of burning rate), and a desire to more accurately simulate the development of the upstream flowfield in an actual motor (which in the limit can only be done by performing actual motor tests). This latter method has the disadvantage that while the erosive burning process is being studied under actual motor conditions, these conditions are difficult to determine accurately. Pressure and velocity vary through the chamber and also change with time. Such burning rate measurement techniques as interrupted burning must use time-averaged values, and the time periods must be relatively long. Continuous measurement of burning rates within a rocket by x-ray requires special elaborate equipment. The use of probes to measure burning rates and pressures is difficult because many probes are required, and also runs the risk of interfering with the chamber flow and disturbing normal burning.

The major drawback of the former method lies in the fact that the level of burning rate augmentation depends not only on the mean crossflow velocity at the point of interest, pressure, and the propellant itself, but also on the influence of the upstream nature of the product gas flow on the local turbulence structure.[5,10] In actual cylindrically perforated motor grain ports, the flow is highly two-dimensional in the forward part of the motor, where inertial terms in the momentum equations describing the flow dominate the viscous terms, leading to the classic "inviscid no slip" velocity profiles described by Culick[11] and measured in cold-flow simulations of cylindrically perforated motors by Yamada and Goto[12] and Dunlap et al.[13] Beddini[8,9] has performed extensive analysis of the development of such flows, obtaining good agreement with the cold-flow experimental work. From his studies he concludes that turbulence first develops in the center of the grain port and eventually works out to the walls (propellant surface), with subsequent development of more nearly classical one-dimensional boundary-layer profiles as the blowing ratio (ratio of radial velocity of products leaving the propellant surface to crossflow velocity) decreases down the motor port. Kutataladze and Leont'ev[14] have developed empirical relationships for the skin friction coefficient in such transpired flows in which, for blowing ratios above a critical value (which depends on several parameters), the boundary layer is considered to be totally blown off the surface (analogous to Beddini's conclusion that a turbulent boundary layer does not exist in the high-blowing-ratio upstream regions of the motor). In Kutataladze's formulation, as in other correlations of blowing effects, as the blowing ratio decreases further below this critical value, the ratio of skin friction to zero-blowing skin friction (for a given crossflow Reynolds number) increases continuously until it approaches a value of unity at very low blowing rates (classic fully developed boundary layer). Obviously, in experiments where product gases are blown across tablets or other small specimens of propellant without the upstream boundary-layer attachment and development phenomena seen in cylindrically perforated (CP) motors (or, even worse, in slots or other complex central port configurations), the turbulence profiles will be different at a given crossflow velocity than in such CP grains. Whether the resultant effects on erosive burning rate at a given pressure and crossflow velocity are first- or second-order is not clear to this author at this time, but it seems highly unlikely that they are totally negligible.

The measurement of erosive burning by use of propellant specimens located outside of a rocket chamber has been investigated by Viles,[15] Zucrow,[16] Vilyunov et al.,[17] Saderholm,[18] and Marklund and Lake,[1] the last authors using two experimental configurations, one with tablets and the other with strips of solid propellant, both positioned inside a tube connected to the exhaust stream of a test rocket. As discussed above, there is considerable question about the nature of the flow across the specimen, but the parameters of mean flow rate, pressure, regression rate, and even temperature are relatively easily measured quite accurately in such a device. Both Viles[15] and Saderholm[18] tested the validity of their data as it pertains to actual motor conditions by calculations of a number of pressure-time curves for motor firings under erosive conditions, using the data obtained from their measurements with externally located samples. Agreement between these calculations and measured pressure-time traces were excellent, leading them to conclude that their experimental procedures for obtaining erosive burning rates were valid.

As indicated above, the use of actual motor tests to determine erosive burning characteristics of propellants has the advantage that the erosion process is being studied under the exact conditions that prevail in a rocket chamber. The disadvantage is that these conditions are difficult to determine accurately. Green,[14] Kreidler,[20] and Peretz[21] have all utilized interrupted burning techniques in studying erosive burning. Ayris and Petrovic[3] have utilized real-time x-ray techniques to study erosive burning in a star-configuration motor, with limited success to date. Strand et al.[22,23] have utilized plasma capacitance gauges to measure erosive burning in CP grain motors, while Traineau and Kuentzman[7] have used ultrasonic burning-rate measurement techniques to study erosive burning in nozzleless motors. Finally, Waesche and O'Brien[24] have evaluated (on paper) various possible techniques, including microwave-Doppler measurements, for continuous measurement of burning rates at various locations along a cylindrically perforated-grain motor.

In addition to experimental studies involving external flow of propellant exhaust gases across tablets or other small propellant specimens (one extreme, yielding relatively inexpensive tests and ease of data analysis, but with major doubts as regards direct relevance to motors as discussed above), and those involving actual use of motors (other extreme, expensive, with difficulty in obtaining accurate measurements), three additional experimental approaches for study of erosive burning, offering compromises between these limits have been employed[25-27] and are briefly described below.

Stokes et al.[25] employed a 50-cm-long slab motor (depicted in Fig. 2) which could be quenched during the early stages of motor operation. This slab motor had a rectangular port with two opposing flat propellant slabs cast into trays, each slab being 2.54-cm wide by 49.2-cm long, with an initial gap between slabs of (typically) 0.7 cm. Rectangular nozzles were sized to give initial port-to-throat area ratios of 1.50, 1.20, and 1.06, corresponding to Mach numbers at the end of the slabs of 0.4–0.7. A liquid quench system was used to extinguish the propellant at 0.05–0.07 s after ignition. Static pressure vs time and total distance burned were measured at five axial locations. A desired form of erosive burning rate expression and one-dimensional compressible flow equations were integrated with various choices of adjustable parameters in the erosive burning rate expression until optimal agreement of measured and calculated pressure-time variation at all

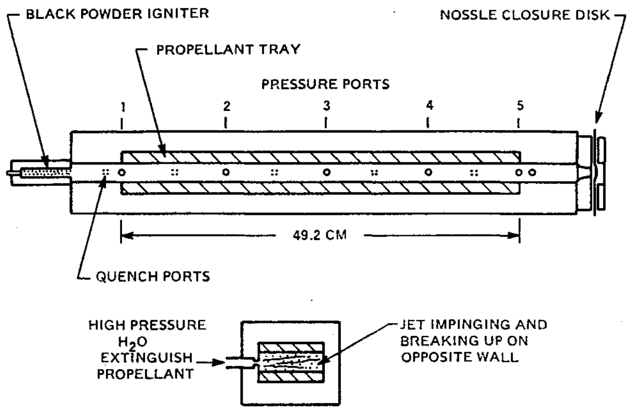

Fig. 2 Slab motor used by Stokes et al.[25] to obtain erosive burning data.

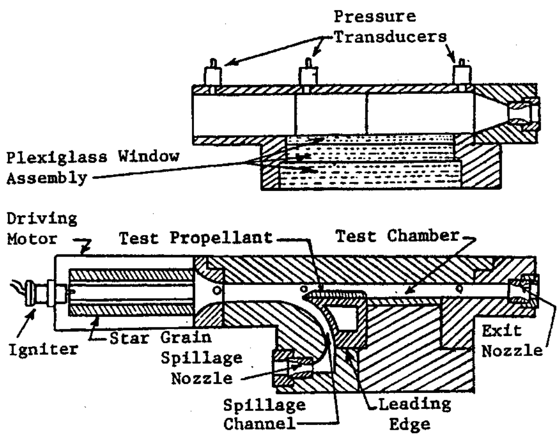

Fig. 3 Schematic diagram of the erosive-burning test apparatus employed by Razdan and Kuo.[26]

measurement locations was obtained. Lack of instantaneous burning rate data necessitated specification of an erosive burning rate expression form (though the form is not restricted as to type), with the measured (post-test) erosion data being used to evaluate unknown constants in the expression for a given propellant and operating pressure.

In the experimental study conducted by Razdan and Kuo,[26] two-dimensional slabs of propellant were utilized in a windowed test chamber with hot combustion products from a "driving motor" flowing over the sample at various velocities (subsonic and supersonic) and chamber pressures (Fig. 3). The test chamber was 39-cm long with a rectangular cross section of 7 × 2.54 cm. This chamber was equipped with a transparent Plexiglas® window assembly composed of an inner sacrificial window, a middle window, and a top window, with the inner window being replaced after each test. The test-propellant sample was clearly visible through this assembly. An interchangeable wedge-shaped steel leading edge was used, with the test propellant sample being glued to the top flat surface of the leading edge, whose length (10.8 cm) allowed development of a turbulent boundary layer over most of the propellant sample (though likely somewhat different in structure from the turbulent boundary layer encountered in an actual motor). The spillage channel depicted in Fig. 3 was used to enable the boundary layer to develop from the beginning of the leading edge. An interchangeable top plate was used to vary channel height, and therefore, gas velocity across the sample. (Pressure gradient could also be varied by use of a tapered top plate.) An interchangeable exit nozzle was used to control pressure (and, in combination with the top plate, velocity in the test chamber). The instantaneous regression rate of the propellant was recorded by a high-speed (1000–1500 frames/s) camera and deduced by means of a motion analyzer.

Details of the experimental device, test procedures, and data analysis procedures (notably used for calculation of burning rate and freestream gas velocity in the test section, not directly measurable) are given in Ref. 26.

The experimental test apparatus and procedures employed by King are described in detail in Ref. 27. A schematic diagram of the basic test apparatus is presented as Fig. 4. A cylindrically perforated 6C4 driver grain (15.2-cm o.d., 10.2-cm i.d.) whose length was chosen to give the desired operating pressure for a given test, produced a high-velocity gas flow through a transition section into a rectangular test section which contained the test grain (generally the same formulation as the driver grain). The contoured transition section was approximately 10-cm long. The test grain extended from the test section back through the transition section to butt against the driver grain in order to eliminate leading-edge effects which would be associated with a test grain standing alone. The test grain was approximately 30-cm long (plus the 10 cm extending through the transition section) by 1.90 × 2.50-cm web and burned only on the 1.90-cm face. The flow channel of the test section was initially 1.90 × 1.90 cm, opening up to 1.90 × 4.45 cm as the test propellant burned back through its 2.54-cm web. For high Mach number tests, the apparatus was operated in a nozzleless mode with the gases choking at or near the end of the test grain, while for lower Mach number tests, a two-dimensional nozzle was installed at the end of the test channel.

During each test, pressure and crossflow velocity varied with time and location along the test grain. (For the nozzleless tests, pressure varied significantly with time and location, while crossflow velocity varied considerably with location, but not significantly with time. On the other hand, for tests using a nozzle with an initial port to throat area ratio of 1.5 or higher, pressure did not vary strongly with location, but did rise with time due to the progressivity of the driver grain, while crossflow velocity varied strongly with time and slightly with location.) These variations permitted design of tests to yield considerable burning rate-pressure crossflow velocity data in relatively few tests, provided that these parameters could be measured continuously at several locations along the test grain. These parameters were measured in the following manner.

The burning rate was directly measured by photographing the ablating grain with a high-speed motion picture camera through a series of four quartz windows located along the length of the test section. Frame by frame analysis of the films permitted determination of instantaneous burning rate to about ±5% resolution as a function of time at each of the four window locations.

For nozzled cases, the measured location of the burning propellant surface at each window as a function of time, together

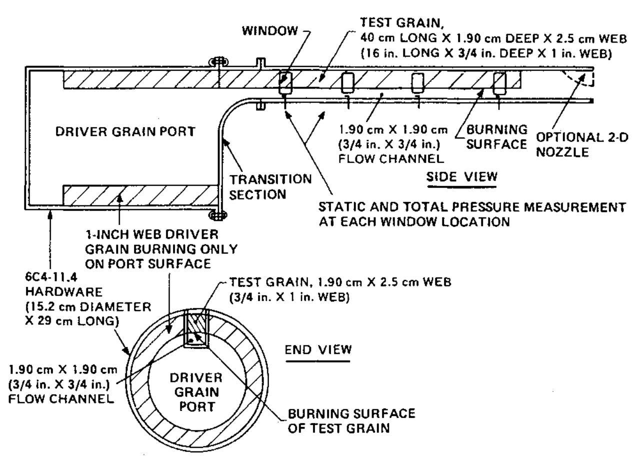

Fig. 4 Schematic diagram of erosive burning test apparatus used by King.[27]

with the known constant throat area, permitted straightforward calculation of the crossflow velocity as a function of time. However, the very sensitive dependence of Mach number on area ratio for $M > 0.5$, made calculation of crossflow velocity from area ratio measurement quite poor for nozzleless cases. Accordingly, for these tests, stagnation pressure was determined at the aft end of the test section and used in combination with the driver chamber pressure for calculation of the stagnation pressure in the test section as a function of time and position. Static pressure wall taps at each window location were used for measurement of static pressure as a function of time for both nozzled and nozzleless cases. From the static and stagnation pressure values determined as a function of time and position down the test section, crossflow Mach number and velocity were calculated as a function of time at each window location in the test section for the nozzleless cases.

In general, studies of the erosive burning of solid propellants have involved use of only one, or at most, two to four different propellants, without study of the effects of systematic variation of propellant compositional and heterogeneity characteristics on sensitivity of burning rate to crossflow velocity. General observations from these studies[1,15-20,28-30] include the following:

1) Plots of burning rate vs gas velocity or mass flux at constant pressure are usually not fitted best by a straight line.

2) Threshold velocities are often (but not always) observed.

3) Occasionally, "negative" erosion rates are observed. (There is some controversy as to the cause, with the thought that in the case of composite propellants it might involve "stifling" of the propellant combustion by flow of melted binder across oxidizer crystals, and that for double-base propellants it might be caused by shearing away of super-rate-producing carbon residues by the crossflow.)

4) Slower burning propellants are more strongly affected by crossflows than higher burning-rate formulations.

5) At high pressure, the burning rate under high crossflow conditions tends to approach the same value for all propellants (at the same flow velocity) regardless of the burning rate of the propellants at zero crossflow. (This observation seems to be refuted by data of King[31-33] presented later in this Paper.)

6) Erosive burning rates do not depend upon core gas temperature of the crossflow (determined from tests in which

Table 2 Propellant matrix (AP composite propellants) tested by King[31-33]

Formulation	Composition	Rationale
4525	73/27 AP/HTPB, 20-μ AP	Baseline formulation, flame temperature = 1667 K
5051	72/27 AP/HTPB, 200-μ AP	Compare with 4525 for AP size effect and base burning rate effect
4685	73/27 AP/HTPB, 5-μ AP	Compare with 4525 and 5051 for AP size effect and base burning rate effect
4869	72/26/2 AP/HTPB/Fe_2O_3, 20-μ AP	Compare with 4525 for base burning rate effect at constant AP size
5542	77/23 AP/HTPB, 20-μ AP	Compare with 4525 for mixture ratio and flame temperature effect at constant AP size, T = 2065 K
5565	82/18 AP/HTPB, 13.65% 90-μ AP, 68.35% 200-μ AP	AP sizes chosen to match base burning rate of 4525. Compare with 4525 for mixture ratio and flame T effect, T = 2575K
5555	82/18 AP/HTPB, 41% 1-μ AP, 41% 7-μ AP	Compare with 5565 for effect of base burning rate
7993	82/18 AP/HTPB, 41% 7-μ AP, 41% 90-μ AP	Further study of AP size and base burning rate effects
7996	82/18 AP/HTPB, 41% 20-μ AP, 41% 200-μ AP	Further study of AP size and base burning rate effects
8019	82/18 AP/HTPB, 27.3% 1 μ, 27.3% 20 μ, 27.4% 200-μ AP	Further study of AP size and base burning rate effects
6626	74/21/5 AP/HTPB/Al, 70% 90-μ AP, 4% 200-μ AP	Same flame T and base burning rate as 5565. Compare with 5565 for Al effect
7523	70/28/2 AP/Polyester/Fe_2O_3, 20-μ AP	Baseline polyester, T = 2250 K, AP size to match BR of 4869, compare for binder effect
7605	78/20/2 AP/Polyester/Fe_2O_3, 23.4% 20-μ AP, 54.6% 200-μ AP	Medium temperature (2800 K) polyester, compare with 7523 and 5542 (latter for base BR effect)

Table 3 Effects of various formulation parameters on sensitivity of AP-composite propellants to crossflow as observed by King[31-33]

Comparison	Parameters studied	Effect on erosive burning
4525, 5051, 4685	Varied d_p, r_0 at fixed binder type, fixed flame temperature	$d_p \downarrow \leftrightarrow r_0 \uparrow \rightarrow \varepsilon \downarrow$
4525, 4869	Varied r_0 at fixed AP size, binder type, and flame temperature	$r_0 \uparrow \rightarrow \varepsilon \downarrow$
4685, 4869	Varied d_p at fixed r_0, binder type, and flame temperature	$d_p \downarrow \rightarrow \varepsilon \downarrow$ Slightly
4525, 5542	Varied O/F[a] ratio (and thus temperature), and r_0 at fixed binder type and AP size	$T_f \uparrow \leftrightarrow r_0 \uparrow \rightarrow \varepsilon \downarrow$
5565, 4525	Varied O/F ratio (and thus temperature) at fixed binder type and r_0	$T_f \uparrow \rightarrow \varepsilon$ Unchanged
5565, 5555, 7993, 7996, 8019	Varied d_p, r_0 at fixed binder type and flame temperature	$d_p \downarrow \leftrightarrow r_0 \uparrow \rightarrow \varepsilon \downarrow$
5565, 6626	Al vs non-Al at fixed r_0, binder type, and flame temperature	Al $\rightarrow \varepsilon$ Unchanged
4869, 7523	Different binder; r_0, d_p held constant; different T (hotter for polyester)	At low P, ε Unchanged At high P, ε Higher for polyester
5542, 7605	Different binder; r_0 held constant; different T (hotter for polyester) and d_p	At low P, ε Unchanged At high P, ε Higher for polyester

Conclusions:

The augmentation factor is strongly dependent on the base burning rate.
There is a small residual effect of oxidizer particle size at fixed base burning rate.
O/F (Flame temperature) affects ε for HTPB systems only through effect on base burning rate.
At fixed base burning rate, aluminum has no effect on ε.
Polyester binder formulations are slightly more sensitive to crossflow than HTPB formulations at fixed base burning rate.

[a]Oxidizer/fuel ratio.

various driver propellant's products are flowed across a given test propellant).

One exception to the statement, that in most studies to date, examination of the effects of systematic variation of propellant parameters (composition, oxidizer particle distribution, etc.) on sensitivity of the propellant to crossflow was not carried out, is the work of King,[31–33] who systematically varied parameters with a series of 11 AP composite propellant formulations, listed in Table 2 (along with rationale for their selection). Detailed results of this test series (carried out in the test apparatus of Fig. 4, described above) will be given in a later section where measured erosive burning rates are compared with predictions of a composite propellant erosive burning model by King. A summary of the observed effects of various parameters on ε (the ratio of burning rate with crossflow to that without it) at constant pressure and crossflow velocity is presented here as Table 3. As observed by previous studies (summarized above), base (no-crossflow) burning rate is seen to have a major effect on crossflow sensitivity, erosive burning ratio increasing with decreasing base rate at fixed pressure.

IV. Empirical Expressions and Relatively Simple Models for Calculation of Erosive Burning Rates

Several empirical expressions for calculation of the ratio of total burning rate (expressed as the sum of zero-crossflow rate plus erosive contribution) of a propellant to the zero-crossflow rate at the same pressure appear in the literature; these generally take one of the following forms:

$$\varepsilon = r/r_0 = 1 + K_1(V - V_t)^m, \qquad m \leq 1 \tag{2}$$

$$\varepsilon = r/r_0 = 1 + K_2(M - M_t)^m, \qquad m \leq 1 \tag{3}$$

$$\varepsilon = r/r_0 = 1 + K_3(G - G_t)^m, \qquad m \leq 1 \tag{4}$$

ε = erosion ratio
r = total burning rate
r_0 = normal burning rate (no crossflow) at the same pressure
K_1, K_2, K_3 = empirical constants
V = crossflow velocity
M = crossflow Mach number
G = crossflow mass flux
m = empirical constant

where the subscript "t" refers to threshold crossflow conditions below which erosion does not occur. (Some propellants have been correlated with nonzero threshold values, while others have been correlated with threshold values set equal to zero.) Effective implementation of such expressions to describe the response of solid propellant burning rates to crossflow, of course requires a fairly extensive data base for each propellant of interest over the range of pressure and crossflow velocity range of interest (extrapolation being quite risky).

Since characterization of a given formulation's burning rate dependency on crossflow at various pressure levels tends to be fairly expensive, a model which permits the designer to predict this dependency without erosive burning testing of various candidate formulations for a given application is highly desirable. In addition, an accurate model which properly accounts for the mechanisms involved in erosive burning can be used by a propellant formulator in developing a formulation which will have desired ballistic properties in a given motor design with a minimum of trial-and-error searching. As a minimum, a model which will permit prediction of erosive burning over a wide range of conditions for a given formulation, given only relatively inexpensive strand-burning data, is highly desirable. Even better would be the ultimate development of a model which would permit prediction of burning rate as a function of pressure and crossflow velocity, given only composition and ingredient size data. Such a model should provide an explanation of the observed burning rate characteristics in the presence of crossflow in terms of the hydrodynamic conditions induced near the propellant surface by the crossflow coupled with the chemical and physical processes which constitute the propellant deflagration mechanism. In the latter area, it appears obvious that different models are required for homogeneous (double-base) and heterogeneous (composite) propellants.

Over the years, a large number of erosive burning models of varying degrees of sophistication have been developed; a list of models examined by this author (with the exception of several complex models utilizing extensive numerical analysis procedures, which are described in the next section) is presented as Table 4. These models mostly fall into one of three categories, as indicated.

Models in the first category are based on the assumption that the erosive burning is driven by increased heat transfer from the mainstream gas flow resulting from the increased mass flux parallel to the grain surface. The best-known and most widely used model, that of Lenoir and Robillard,[34] falls into this category. Since this model is the one most widely used today by motor designers (actually it is a "data fitting" tool, requiring experimental data for each new formulation, rather than a true predictive model), it will be discussed in more detail than the others. In this model, the authors state that the total burning rate (r) is the sum of two effects: 1) a rate dependent on pressure (r_0, the normal burning rate), and 2) a second erosive rate (r_e) dependent upon the combustion gas flow rate. This equation entails an assumption that the pressure dependent "base" rate, r_0, is unaffected by an increase in total rate at a given pressure, an assumption which almost certainly cannot be true. This problem has been discussed in detail by King,[47] with derivation of a modified Lenoir and Robillard[34] expression allowing for the coupling of flame standoff distance with burning rate. While Lenoir and Robillard[34] assume $r = r_0 + r_e$, allowance for the coupling effect results in $r = (r_0^2/r) + r_e$. In physical terms, Lenoir and Robillard have failed to account for the fact that the increased burning rate caused by erosive feedback at constant pressure results in the propellant flame being pushed further from the surface, decreasing its heat feedback rate and, thus,

Table 4 General categories of models of erosive burning described briefly in Sec. IV

Models based on augmented heat transfer from the "core gas" in the presence of crossflow
Lenoir and Robillard[34]
Zucrow et al.[35]
Saderholm[18]
Marklund and Lake[1]
Models based on alteration of transport properties in the region between the flame zone(s) and the propellant surface by crossflow
Saderholm et al.[36]
Lengelle[37]
Corner[38]
Vandenkerchove[39]
Zeldovich[40]
Vilyunov[17]
Geckler[41]
Parkinson et al.[5,6,42]
Models based on chemically-reacting boundary-layer theory
Tsuji[43]
Miscellaneous
Klimov[44]
Molnar[45]
Miller[46]

decreasing the propellant burning rate part of the way back toward the base rate.

A more general weakness of models in the first category is that these models predict substantial dependence of erosive burning on the temperature of the core gas; such dependence was found by Markland and Lake[1] in experiments with propellant tablets exposed to crossflow products from motors operating at different flame temperature (1700 and 2400 K), and later by King[48] in the test apparatus of Fig. 4 described earlier (with driver propellants with flame temperatures of 1667 and 2425 K) to be completely absent. (The Lenoir and Robillard model predicts that the erosive contribution should be 50% higher with the higher temperature driver in each case, as discussed in detail in Refs. 27 and 48.) This observed lack of dependence of erosive burning rate on core gas temperature tends to indicate that all models in the first category in Table 4 are on shaky grounds.

The model of Zucrow et al.[35] is worthy of particular attention, since it is the only model known to this writer which permits prediction of negative erosion which has been observed in some cases. However, it may be shown that this prediction results from a physically impossible result of a mathematical extrapolation. The basic burning rate expression employed is

$$r = r_0 + h(T_{\text{combustion}} - T_{\text{surface,avg.}})/Q\rho_{\text{prop}} \tag{5}$$

where Q is basically the heat required to preheat and vaporize unit mass of the propellant (with some corrective adjustments), and h is the heat transfer coefficient from the core gas to the propellant surface. Ancillary expressions used include

$$h = h_0(C_h/C_{h0}) \tag{6}$$

$$C_h/C_{h0} = 1 - \beta_T B \tag{7}$$

$$B = \rho_{\text{prop}} r_0/C_{h0}G \tag{8}$$

where β_T is a constant transpiration parameter, and C_{h0} and h_0 are the Stanton number and the heat transfer coefficient in the absence of blowing, all other parameters being as defined earlier.

The difficulty lies in the use of Eq. (7) for the ratio of the Stanton number with crossflow, to that without crossflow. This expression should only be used for values of $\beta_T B \ll 1$. As it is, at sufficiently small values of G, B exceeds $1/\beta_T$. When this occurs, Eq. (7) yields a negative value for the Stanton number (violating the second law of thermodynamics), and therefore, h becomes negative, as does the second term of Eq. (5), resulting in a predicted burning rate, r, less than the burning rate in the absence of crossflow, r_0. The correct limit for C_h/C_{h0} as $G \rightarrow 0$ ($B \rightarrow \infty$) is zero, while Eq. (7) predicts it to go to minus infinity.

The models of Saderholm[18] and Marklund[1] are not vastly different from that of Lenoir and Robillard,[34] except that Saderholm totally ignores the base (no crossflow) burning rate in comparison to the erosive contribution, a treatment that seems a bit drastic, particularly for fairly low crossflow velocities.

The second category of models listed in Table 4 includes models based on the alteration of transport properties in the region between the gas flame and the propellant surface by the crossflow, generally due to turbulence effects. Included in this category are models in which the thermal conductivity in this region is raised by turbulence, and models in which the time for consumption of fuel gas pockets leaving the surface is reduced by the effects of turbulence on diffusivity. Four of these models were developed for double-base propellants. In three of these (the models of Corner,[38] Zeldovich,[40] and Vilyunov[17]), the basic approach is to calculate, using various boundary-layer hydrodynamic models, an effective ratio of turbulent thermal conductivity (or diffusivity) to laminar conductivity and relate this to increased flux to the propellant surface from the gas flame and, thus, to increased rate of ablation of the propellant surface. The Vandenkerchove[39] model, however, is somewhat different. In this model, he assumes that the key heat transfer driving temperature is achieved at the inner edge of the fizz zone. He then assumes that in cases where, in the absence of crossflow, this fizz zone would begin at a distance from the surface greater than the distance from the surface to the edge of the laminar sublayer (calculated from a universal u^+, y^+ correlation approach) with crossflow, this edge of the fizz zone will be fixed by the edge of the laminar sublayer. Whenever this is the case, the resultant "flame" position will be closer to the surface than without crossflow, the resultant heat flux (calculated as the ratio of the thermal conductivity to the flame offset distance) will be higher, the propellant surface temperature will increase, and the propellant ablation rate will become higher. Since the laminar sublayer thickness decreases with increasing crossflow velocity, the burning rate will also increase with this parameter.

The models of Lengelle[37] and Saderholm et al.[36] for composite propellant erosive burning are somewhat similar in principle, though the latter model is applied to the special case of very fuel-rich propellants at quite low crossflows. The basic propellant combustion mechanism assumed is the granular diffusion model in which pockets of fuel vapor leave the surface and burn away in an oxidizer continuum at a rate strongly dependent upon the rate of micromixing of the oxidizer vapor into the fuel vapor pocket. The driving mechanism by which the crossflow is assumed to increase the burning rate is through increased turbulence associated with increasing crossflow raising the turbulent diffusivity in the mixing region (thus increasing the rate of mixing and decreasing the effective distance of the diffusion flame from the surface), and raising the effective turbulent thermal conductivity. Both the decrease in distance from heat release zone to surface and the increase in thermal conductivity increase the heat flux to the surface, thus causing the propellant to ablate more quickly. There are several notable weaknesses associated with the Lengelle model: 1) the granular diffusion flame model is not physically realistic; 2) the AP monopropellant flame is ignored; and 3) the boundary-layer treatment used to calculate the dependence of the effective turbulent diffusivity and conductivity on the crossflow is unrealistic in its use of a power velocity law all the way from the freestream to the surface.

In the more recent studies of Parkinson et al.,[5,6,42] only alteration of the effective thermal conductivity between the propellant gas flame zone and the surface by crossflow-induced turbulence is considered as a driving mechanism for erosive burning. In their first work,[42] the authors use blown-boundary-layer theory to calculate the Stanton number (controlling heat feedback) as a function of the skin friction coefficient in the presence of blowing, utilizing expressions based on the work of Kutataladze and Leont'ev[14] for calculation of this coefficient. They then use the calculated Stanton number for comparison of the heat feedback rate from the gas flame to the surface with that based on pure conduction (no crossflow case), allowing for the fact that increased burning rate will push the flame zone further away from the surface (under their assumption that the "delay time" of the reaction is not affected by the turbulence) in arriving at an expression for the total burning rate as a function of the no-crossflow rate and the Stanton number. In their two subsequent papers,[5,6] they expand their analysis to include treatment of the laminar sublayer thickness relative to the flame standoff distance, and modify their blown-boundary-layer analysis to allow the skin friction factor to only asymptotically approach zero at high blowing rates, rather than being identical to zero at blowing ratios (blowing rate/crossflow rate) greater than a critical value (Kutataladze approach).

Only one model[43] is listed in the third category of Table 4; however, further modeling efforts in this category, of considerably greater complexity, are discussed in the next section. Unfortunately, the Tsuji[43] study is not particularly useful, due to the assumption of a totally laminar boundary layer and limitation to a situation where the freestream velocity is proportional to the distance from the head-end of the grain. Other simplifications include assumption of premixed stoichiometric fuel and oxidizer (rendering the model inapplicable to composite propellant systems) and use of one-step global kinetics.

In the "miscellaneous" category of Table 4, the Klimov[44] model is mainly aimed at calculation of threshold crossflow velocities (below which the propellant is unaffected by crossflow). Klimov claims that the threshold velocity is the mainstream crossflow velocity above which the "turbulence front" subsides onto the propellant surface (recall the earlier mention of Beddini's work[8,9] supporting this hypothesis), and presents boundary-layer analysis procedures for calculating this threshold velocity as a function of the transpiration (blowing) velocity of gases ablating from the propellant surface. In addition, he postulates that negative erosion is due to "stirring up" of cool streams of binder decomposition products over the oxidizer surface, leading to intensification of their cooling effect and to screening of heat feedback from oxidizer/fuel diffusion flames.

Molnar's model,[45] developed for homogeneous propellants with a laminar crossflow, is based on an assumption (which does not appear to this author to be realistic) that the lateral velocity gradient at the burning surface governs erosive burning. Miller[46] assumes that the time for a unit of propellant mass to be consumed is a linear sum of a chemical reaction time and "the time required for turbulent transport of heat to the propellant surface"; such an additivity approach seems quite unrealistic.

V. Complex Numerical Analysis Erosive Burning Models

Modeling efforts in this area include those of Beddini,[8-10] with major emphasis on fluid dynamic aspects, but a very oversimplified unrealistic treatment of solid propellant combustion itself; composite propellant[49-51] and double-base propellant[52] models by Kuo et al., with emphasis on flow dynamic aspects, but also with inclusion of treatment of combustion processes; a "first-generation" composite propellant model,[27,48,53] "second generation" composite propellant model,[31,32,54] and a double-base propellant model[55,56] by King (with more emphasis on combustion mechanism details coupled with a more empirical treatment of fluid dynamic aspects); and a composite propellant model by Renie et al.[57-59] which is similar to and derivative of the King second-generation composite model, and accordingly will not be discussed in detail. Godon et al.[60,61] have recently presented/published two papers on modeling of erosive burning of composite propellants, culminating in a formulation which they refer to as their "concise model," discussed in detail in Ref. 61. There are considerable similarities in the approaches of King, Renie, and Godon, particularly in treatment of the fluid dynamic aspects of the problem. As will be discussed later, the King second generation composite propellant combustion modeling approach includes two mechanisms for burning rate augmentation by crossflow, bending of a columnar diffusion flame by that crossflow, and augmentation of mixing/heat transport by crossflow-induced turbulence, while the other two sets of modelers include only the latter mechanism. However, as will be discussed later (and probably not sufficiently emphasized in King's publications) virtually all of the burning rate augmentation predicted by the second generation model results from the latter mechanism, with flame bending playing, at most, a secondary role. The models of these three investigators also differ in their treatment of gas-flame details. Though all consider columnar diffusion flames, the treatment of heat release distributions within these flames differ in detail; however, these differences are probably, at most, second-order in their effects on erosive burning predictions. Due to the general similarity of the modeling by these three sets of investigators, only the model of King (among these three) will be described in detail, while the Beddini and Kuo models, due to major differences in approach, will be outlined below. It should be noted that even the models emphasizing fluid dynamic aspects of erosive burning are limited to simple configurations and do not deal with slots, stars, or other irregular perforations (often used in practical motors) which generally result in highly three-dimensional flows.

A. Beddini Modeling Efforts

Beddini[8-10] has carried out what is probably the most realistic and thorough analysis of the flow structure (including turbulence) involved in the erosive burning of solid propellants in either two-dimensional slab configurations or in the port of a cylindrically perforated motor, employing second-order closure turbulence analysis procedures. With his approach, he has been able to predict flow development structures consistent with those measured by Yamada and Goto[12] in cold-flow studies simulating blowing-wall rocket motors ports, structures considerably different from those predicted using more standard k-ε developing turbulent boundary-layer analyses, such as those employed by Kuo and coworkers,[49-52] discussed later. However, his combustion model is highly idealized (not representative of actual flame structures in either composite or double-base propellant combustion)—consequently, it is concluded that his results are mainly of use for trend analysis (e.g., scaling of threshold effects, an important area of interest in itself) rather than for prediction of the erosive burning characteristics of specific propellants.

B. Modeling Efforts of Kuo and Coworkers

Kuo[49] and coworkers present an analysis of erosive burning of composite propellants in the geometry of their test apparatus (described earlier), a flat-plate with a fixed leading edge. In this work, they perform a parabolic turbulent boundary-layer analysis using a k-ε model for closure of their turbulent equations. (In standard fashion, they begin with general unsteady-state conservation equations for mass, momentum, fuel, oxidizer, enthalpy, etc., replace the instantaneous variables with mean plus fluctuating components, and time-average the resulting equations, leading to a number of $\overline{X'Y'}$ crossproducts which must be correlated for closure of the problem.) In the near-wall region, they utilize a modified Van Driest[62] turbulent viscosity formulation, with inclusion of a term based on the work of Cebeci and Chang[63] to account for wall roughness, for calculation of turbulent kinetic energy and dissipation. In their analysis, they assume that the heat release at any point in the gas phase is controlled by eddy breakup, which is proportional to the square root of local turbulent kinetic energy level and to the radial gradient of unburned fuel concentration. Among other simplifications regarding the combustion processes, they assume infinite kinetics for the oxidizer/fuel flame, neglect molecular diffusion as regards to mixing, and neglect the gas-phase ammonium perchlorate monopropellant flame, considered by most modelers of composite propellant combustion to be an important factor. In solving their equations, the authors employ a standard Patankar-Spalding numerical approach, marching along the grain from the leading edge (parabolic problem).

In Ref. 50, the previous model is extended to treatment of erosive burning in the port of a cylindrically perforated propellant grain; in this study, both the developing (inviscid core flow) and fully developed regions of the flow are considered. The marching analysis is initiated at the point where the boundary layer starts to develop (though it is not clear how the authors decide where this is). In general, the analysis is quite similar to that used for the flat-plate analysis except for addition of treatment of axial pressure gradients associated with flow acceleration down the bore. In Ref. 51, the analysis is further extended to formulations containing HMX and aluminum, as well as ammonium perchlorate and binder, with treatment of the species formed by reaction of ammonium perchlorate and binder as an "equivalent oxidizer" and those formed by HMX and aluminum as "equivalent fuel," a somewhat questionable concept.

Comparison of theoretical results predicted using the flat-plate analysis with experimental results obtained by the Penn State investigators[26] shows close agreement. From the results of this study, the authors conclude that the mechanism of erosive burning is increased turbulence activity near the regressing propellant surface with increased crossflow velocity. Both experimental and theoretical results indicate that erosive burning is more pronounced at higher pressure; in addition, erosive burning rate in a rocket motor is predicted to decrease with increasing port diameter, in agreement with observations of many investigators in scale-up studies and motor development programs.

There appear to be some major difficulties with the modeling approach described above, in that the modelers appear to be discarding mechanisms which determine burning rate in the absence of strong crossflow. At very high turbulence levels associated with high crossflows, leading to erosive burning ratios far greater than unity, this neglect might be acceptable. However, at lower levels of crossflow, where the erosive burning ratio is not far from unity (e.g., less than 2), it seems obvious that both erosive and nonerosive mechanisms must contribute to the total burning rate in that nature, in general, does not permit discontinuous changes from all one mechanism to all another with small changes in the parameter affecting their relative significance. (That is, it is very difficult to see how mechanisms determining the zero-crossflow rate disappear as soon as the total rate rises several or even tens of percent above this zero-crossflow rate.) Basically, the model appears to have a major deficiency resulting from the assumption that the heat release from an oxidizer/fuel gas flame is totally controlled by eddy breakup, with the result that in the absence of crossflow-induced turbulence, no contribution to the propellant ablation is made from O/F gas flame heat feedback. (As turbulent kinetic energy goes to zero in this model, eddy breakup goes to zero and, with neglect of molecular diffusion mixing processes, mixing and reaction also go to zero.) Thus, in the absence of crossflow, this model requires that all heat necessary for preheating and vaporizing the propellant ingredients at the observed zero-crossflow rate must be supplied by surface/subsurface heat release and/or a collapsed ammonium perchlorate monopropellant flame, a scenario considered unrealistic by modern modelers. (That is, the O/F flame in modern ammonium perchlorate composite propellant models is calculated to make an important contribution to the surface heat balance at zero crossflow under all reasonable pressure conditions—in fact, the dependence of zero-crossflow burning rate on oxidizer particle size results from the importance of the O/F flame.)

Another area of major difficulty with the motor port grain model lies in the use of a one-dimensional inviscid core flow plus boundary-layer approach at and near the head end of the grain port. As has been shown experimentally by Yamada and Goto[12] and Dunlap et al.,[13] and analytically by Beddini[8–10] among others (as discussed earlier), the entire flow near the head-end of a perforated grain port must be highly two-dimensional, precluding use of such an analysis. Only at a distance a considerable number of diameters downstream of the motor head-end, where the ratio of blowing velocity to crossflow velocity has dropped below a critical value (as the crossflow velocity builds up), is such an analysis applicable. In the upstream regions, the highly two-dimensional nature of the flow results in near-wall turbulence intensities being quite small compared to those that would be predicted by the analysis of Kuo and coworkers.[49,50] As a result, as discussed by Beddini, erosive effects in the upstream regions of perforated grains should be considerably less than predicted by this analyses.

In Ref. 51, Kuo and coworkers present a model of erosive burning of double-base propellants; analysis of the flow is similar to that for their composite propellant modeling. In this study, the authors do treat multiple reaction zones, observed in the combustion of double-base propellants. Again, however, in calculation of heat release rates in these zones, the authors assume that these are controlled by eddy breakup, in this case involving the mixing of "lumps" of unburned and fully burned gases. Accordingly, the heat release rate again goes to zero as turbulent kinetic energy goes to zero, since they have once more neglected molecular diffusion mixing processes—therefore, this model too is suspect for crossflows not leading to high erosive burning ratios, since it cannot give the correct zero crossflow burning rate limit, a minimum requirement for a realistic erosive-burning model as discussed above.

C. Modeling Efforts of King

1. First-Generation Composite Propellant Model

The first-generation composite propellant erosive burning model by King[27,48,53] is based on a hypothesis that augmentation of burning rate by crossflow is caused solely by the bending of columnar diffusion flames (involving reaction of ammonium perchlorate and binder decomposition products), with resultant movement of this O/F flame closer to the surface, causing increased heat feedback flux; affects of crossflow-induced turbulence on transport properties is not considered. Although this model does yield good predictive capability for erosive burning rates, it requires physically unrealistic values of some of the parameters grouped in three constants used to fit zero-crossflow burning rate data (an integral part of the procedure). Accordingly, this model was eventually discarded by the author in favor of a more fundamental second-generation model (presented in the next section) in which both zero-crossflow and erosive burning rates are predicted from first principles, and in which both flame-bending and turbulence-augmented transport property mechanisms are included. However, for sake of completeness, a brief description of the first-generation model is included here.

A schematic diagram depicting the first generation composite propellant erosive-burning model is presented in Fig. 5. In the first part of the figure, the flame processes occurring in the absence of crossflow are depicted. There are two flames

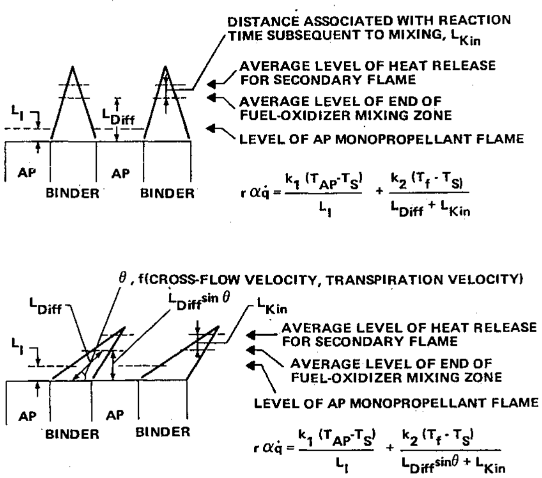

Fig. 5 Sketch of King first-generation model postulated erosive burning mechanism: a) no crossflow velocity and b) crossflow, L_{Kin}, L_{Diff}, $L_I = f(\dot{m}, P)$ alone, independent of crossflow angle.

considered: 1) an ammonium perchlorate deflagration monopropellant flame close to the surface; and 2) a columnar diffusion flame resulting from mixing and combustion of the ammonium perchlorate deflagration products and fuel binder pyrolysis products at an average distance somewhat further from the surface. Three important distance parameters considered are 1) the distance from the propellant surface to the "average" location of the kinetically controlled ammonium perchlorate monopropellant heat release (L_I); 2) the distance associated with mixing of the oxidizer and fuel for the diffusion flame (L_{Diff}); and 3) the distance associated with the fuel-oxidizer reaction time subsequent to mixing (L_{Kin}). (An alternate way of thinking about this last distance, which is difficult to show in the figure, is to picture two stacked cones in the figure, separated by the distance L_{Kin}.) A heat balance between heat feedback from these two flames and the energy requirements for heating the propellant from its initial temperature to the burning surface temperature and decomposing it yields (assuming that the heat feedback required per unit mass of propellant consumed is independent of burning rate)

$$r \propto \dot{q}_{\mathrm{feedback}} \propto k_1(T_{\mathrm{AP}} - T_s)/L_I + k_2(T_f - T_s)/(L_{\mathrm{Diff}} + L_{\mathrm{Kin}}) \tag{9}$$

(The rationale leading to this type of summing of feedback contributions from the two different flames is discussed in detail in Ref. 53.)

The situation pictured as prevailing with a crossflow is shown in the second part of Fig. 5. Since L_I and L_{Kin} are both kinetically controlled and are, thus, simply proportional to a characteristic reaction time (which is assumed to be unaffected by the crossflow) multiplied by the propellant gas velocity normal to the surface (which for a given formulation is fixed by burning rate and pressure alone), these distances are fixed for a given formulation at a given burning rate and pressure, independent of the crossflow velocity. Of course, since crossflow velocity affects burning rate at a given pressure through its influence on the diffusion process as discussed below, L_I and L_{Kin} are influenced through the change in burning rate, but this is simply coupled into a model by expressing L_I and L_{Kin} as explicit functions of burning rate and pressure in that model. The important point is that they can be expressed as functions of these two parameters alone for a given propellant.

However, the distance of the effective mixing zone height from the propellant surface is directly affected by the crossflow. To a first approximation, L_{Diff} measured along a vector coincident with the resultant and crossflow velocities should be the same as L_{Diff} normal to the surface in the absence of a crossflow at the same burning rate and pressure. A simplified version of the reasoning leading to this conclusion is presented in Fig. 6, which is essentially self-explanatory. While the time required for a parcel leaving the surface to travel the distance L_{Diff} in the flow direction θ at constant burn rate is inversely proportional to the sine of the flow angle, the characteristic mixing time is also decreased, since the average concentration gradient is increased by the circular cross section (in the absence of crossflow) being converted to an elliptical cross section with major axis d_p (oxidizer particle diameter) and minor axis $d_p \sin\theta$. Doing an exact calculation of the effect on characteristic mixing time is somewhat difficult: however, replacement of the circle diameter d_p by the geometric mean ellipse diameter $(d_p \cdot d_p \sin\theta)^{1/2}$ in calculating concentration gradients does not seem unreasonable. When this is done, the magnitude of L_{Diff}, measured in the flow direction, is calculated to be independent of flow angle, θ, as shown in Fig. 6. [A somewhat more rigorous (and immensely more complex) analysis has been performed, indicating that the above approximation is quite good for $\theta > 20$ deg, but that for smaller angles (columns further pushed over), the magnitude of L_{Diff} actually begins to decrease relative to the no-crossflow value.]

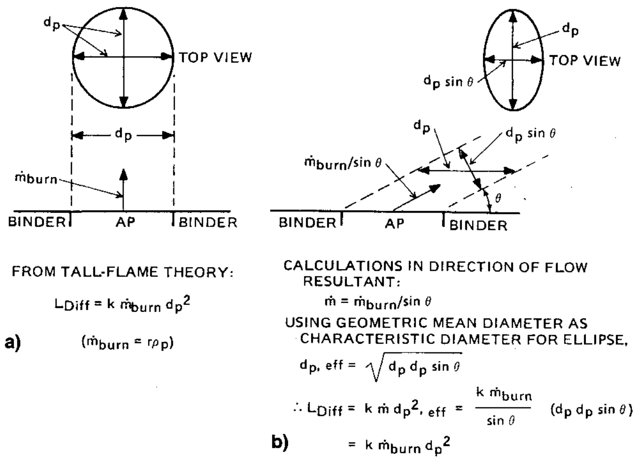

Fig. 6 Procedure for calculation of dependency of diffusion distance on flow angle: a) no crossflow and b) crossflow, with net resultant flow at angle θ.

At any rate, to a reasonably good approximation, the magnitude of L_{Diff} is independent of the crossflow velocity (at fixed pressure and burning rate), although its orientation is not. Thus, the distance from the surface to the average mixed region is decreased to $L_{\mathrm{Diff}} \sin\theta$ (Fig. 5). The heat balance at the propellant surface now yields

$$r \propto \dot{q}_{\mathrm{feedback}} \propto k_1(T_{\mathrm{AP}} - T_s)/L_I + k_2(T_f - T_s)/(L_{\mathrm{Diff}} \sin\theta + L_{\mathrm{Kin}}) \tag{10}$$

This picture was used as the basis of development of the first generation flame bending model for prediction of burning rate vs pressure curves at various crossflow velocities, given only a curve of burning rate vs pressure in the absence of crossflow. The general approach utilized in development of this model follows:

1) The expressions for L_I, L_{Diff}, and L_{Kin} as functions of burning rate (or $\dot{m}$), pressure, and propellant properties are derived and substituted into a propellant surface heat balance.

2) The resulting equation is worked into the form of Eq. (16) (developed in succeeding paragraphs) for burning in the absence of crossflow. A regression analysis using no-crossflow burning rate data is performed to obtain best fit values for A_3, A_4, and A_5, three constants appearing in this expression. (d_p is the average ammonium perchlorate particle size. For a given propellant, the burning rate data may be just as effectively regressed on A_3, A_4, and $A_5 d_p^2$, eliminating the necessity of actually defining an effective average particle size.)

3) From these results, expressions are obtained for L_I, L_{Diff}, and L_{Kin} as functions of burning rate (or $\dot{m}$) and pressure.

4) These expressions are combined with an analysis of the boundary-layer flow (which gives the crossflow velocity as a function of distance from the propellant surface, mainstream velocity, and propellant burning rate) to permit calculation of the angle θ (Fig. 5), L_I, L_{Diff}, L_{Kin}, and $\dot{m}$ for a given pressure and crossflow velocity.

In the derivation of burning rate for a composite propellant in the absence of a crossflow, an energy balance at the propellant surface was written as (Fig. 5)

$$\lambda_A(T_f - T_s)/(L_{\mathrm{Diff}} + L_{\mathrm{Kin}}) + \lambda_B(T_{\mathrm{AP}} - T_s)/L_I = \dot{m}[c_p(T_s - T_0) + Q_{\mathrm{VAP}} - Q_{\mathrm{RX}}] \tag{11}$$

where T_0 is the bulk propellant temperature, and Q_{VAP} and Q_{RX} are heat sink and source terms in the solid propellant. The first term in this equation represents heat flux from the final flame to the surface, the second represents heat flux from the ammonium perchlorate monopropellant flame, and the third represents the heat flux requirements for ablation of the propellant at $\dot{m}$. (Several simplifying assumptions were utilized in writing of the equation in this form, as discussed in detail in Ref. 53).

The monopropellant ammonium perchlorate flame offset distance, L_I, may be expressed as the product of a characteristic reaction time, τ_I, and the linear velocity of gases leaving the propellant surface:

$$L_I = \tau_I \dot{m}/\rho_{\text{gas}} \tag{12}$$

For a second-order gas-phase reaction (generally assumed), τ_I is inversely proportional to pressure, and for a given formulation, the gas density is directly proportional to pressure, yielding

$$L_I = K_1 \dot{m}/P^2 \tag{13}$$

A similar analysis for L_{Kin} yields:

$$L_{\text{Kin}} = K_2 \dot{m}/P^2 \tag{14}$$

For a columnar diffusion flame, it may easily be shown that the diffusion cone height, L_{Diff}, may be expressed as

$$L_{\text{Diff}} = K_3 \dot{m} d_p^2 \tag{15}$$

Equations (11) and (13–15) may be combined to yield

$$r = \dot{m}/\rho_s = A_3 P[1 + A_4/(1 + A_5 d_p^2 P^2)]^{1/2} \tag{16}$$

Burning rate vs pressure data for a given propellant in the absence of a crossflow may then be analyzed by means of a fairly complicated regression analysis procedure to yield values of the constants A_3, A_4, and A_5 (or $A_5 d_p^2$) for that given propellant. The constants K_1, K_2, and K_3 are related to these constants in turn by

$$K_1 = (T_{\text{AP}} - T_s)\lambda_B/(A_2 A_3^2 \lambda_A) \tag{17}$$

$$K_2 = (T_f - T_s)/(A_2 A_3^2 A_4) \tag{18}$$

$$K_3 = (T_f - T_s)A_5/(A_2 A_3^2 A_4) \tag{19}$$

where

$$A_2 = \rho_s^2[c_p(T_s - T_0) + Q_{\text{VAP}} - Q_{\text{RX}}]/\lambda_A \tag{20}$$

Data of Mickley and Davis[64] were used to develop empirical expressions for the local crossflow velocity as a function of distance from the propellant surface, mainstream crossflow velocity, and transpiration rate (gas velocity normal to the propellant surface). In this analysis, it was decided that the transpiration velocity should be calculated as the gas velocity normal to the surface at the final flame temperature. (Mickley and Davis correlations are based upon the ratio of mainstream velocity to transpiration velocity.)

The analyses described above were used in derivation of eight equations in eight unknowns for the burning of a given composite propellant at a given crossflow velocity; a computer code was developed to solve this equation set, yielding a predicted burning rate for a given pressure, crossflow velocity, and set of constants A_3, A_4, and $A_5 d_p^2$ obtained from regression of no-crossflow data for that propellant. Details appear in Ref. 53. As mentioned earlier, this model was used to successfully predict erosive burning rates for a number of composite propellants over a wide range of pressures and crossflow velocities; however, examination of some of the intermediate parameters for calculation of the various distance parameters indicated physically unrealistic values. Accordingly, this model was abandoned in favor of a more fundamental second-generation model, described in the next section.

2. Second-Generation Composite Propellant Model

King's second-generation erosive burning model for composite propellants[31,32,54] is built on a zero-crossflow composite-propellant burning model, also developed by King,[65] which is, in turn, loosely based on the classic Beckstead-Derr-Price (BDP) model[66] (though with many major and minor modifications as described in detail in Ref. 65). Both two-dimensional and axisymmetric versions of this erosive burning model were developed; the version described in the following paragraphs was developed for the two-dimensional slab geometry employed in the previously described experimental program conducted by King. The version for treatment of cylindrically-perforated grain ports was developed by way of straightforward modifications to the two-dimensional model version, with the main modifications involving a change in zero-blowing skin friction coefficient expressions and modification of the momentum integral equation used in calculation of local shear stress as a function of distance from the propellant surface, and will not be discussed further. A relatively brief description of the two-dimensional model is presented below; for further details, the reader is directed to Refs. 31, 32, 54, and 65.

The basic model centers around an energy balance, the product of burning mass flux and energy requirements to raise ingredients from ambient to surface temperature (related to burn rate by an Arrhenius function) and vaporize that fraction not consumed in subsurface reactions being equated to the sum of heat release rate from subsurface reactions and heat feedback rates from two gas flame zones (Fig. 7). Thus, burning rate is controlled by three heat release zones: 1) a thin subsurface zone; 2) a gas-phase AP decomposition product monopropellant flame; and 3) a diffusion flame between AP products and binder pyrolysis products.

Subsurface heat release is calculated using an estimated subsurface temperature profile substituted into a rate expression representing subsurface heat release data measured by Waesche and Wenograd.[67] This expression is integrated from the surface to a depth where the temperature equals the AP melting point to obtain total subsurface heat release. This procedure differs from the BDP approach, in which subsurface heat release per unit mass of propellant is assumed constant, independent of burning rate.

For the gas phase, a two-flame approach was chosen (in contrast to the three-flame approach of BDP), the flames being an AP monopropellant flame and a columnar diffusion[68] flame. Three distances (FH90 sin θ, L_{AP}, and L_{RX}) are important in determining heat feedback from these flames (Fig. 7). FH90 is a distance associated with 90% mixing of fuel and oxidizer gases, while L_{RX} and L_{AP} are reaction distances (products of gas velocity normal to the surface and reaction times) associated with diffusion and monopropellant flames, respectively. As discussed in the previous section, describing King's first-generation model, crossflow-induced flame bending is postulated to reduce the mixing region height by the factor sin θ, where θ is determined by the resultant of local transpiration and crossflow velocities. AP monopropellant flame heat release is assumed to occur at one plane, while the dif-

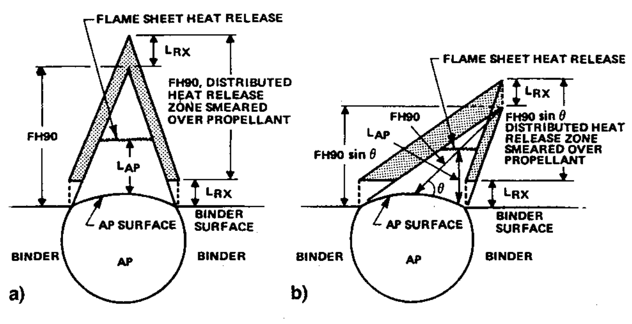

Fig. 7 Schematic of postulated composite propellant flame structure, with and without crossflow: a) no crossflow case and b) crossflow case.

fusion flame releases heat in a distributed fashion (defined by a Burke-Schumman[68] analysis), between distances L_{RX} and L_{RX} + FH90 sin θ from the surface.

Details of equation development for the unimodal oxidizer nonmetallized propellant model appear in Refs. 54 and 65. Included in this model are three "free" constants (pre-exponentials associated with the subsurface rate expression and two rate expressions used to calculate gas-phase reaction times). Optimized values for these constants were chosen using zero-crossflow burning rate data for four unimodal oxidizer AP/HTPB (hydroxy-terminated polybutadiene) formulations, and subsequently used in all other calculations.

The model was extended to multimodal oxidizer formulations using a variation of Glick's "petit ensemble" approach.[69] First, a multimodal oxidizer formulation is divided into subpropellants, each containing oxidizer of one size. These subpropellants are assumed to burn noninteractively, with the unimodal model being used to calculate individual mass fluxes. Oxidizer of one size is allowed to affect another subpropellant's burning rate only through possible influence on the assignment of fuel to that subpropellant. Unequal oxidizer/fuel ratios for the subpropellants are permitted by

$$V_{f,\mathrm{di}} = C_2(D_{0,i})^{\mathrm{XEXPOF}} \tag{21}$$

where $V_{f,\mathrm{di}}$ is the fuel volume assigned to a particle of diameter $D_{0,i}$, XEXPOF is an arbitrary constant, and C_2 is fixed by overall continuity. (XEXPOF = 3 results in equal oxidizer/fuel ratios for each subpropellant, while XEXPOF < 3 results in subpropellants with small oxidizer being more fuel-rich than those with large oxidizer. XEXPOF = 3 was used in the following calculations.) In averaging the individual subpropellant fluxes, Glick assumes that the average fractional surface area associated with subpropellant i is equal to its overall volume fraction. Critical analysis indicates, however, that if the subpropellants burn at different rates, slower burning ones will occupy a disproportionately higher fraction of surface. Development of this concept for XEXPOF = 3 leads to

$$\bar{r} = 1/\Sigma(x_i/r_i) \tag{22}$$

replacing Glick's expression

$$\bar{r} = \Sigma x_i r_i \tag{23}$$

r_i = burning rate of subpropellant i
x_i = mass fraction of overall propellant in subpropellant i
$\bar{r}$ = average burning rate

The original model was also extended to treat metallized propellants. The metal (aluminum) is allowed to alter burning rate through heat sink effects and by conductive and radiative feedback from burning metal particles. Phenomena treated included agglomeration, particle velocity lags, ignition delay, particle combustion, conductive feedback from multiple heat release zones, and radiative feedback. For multimodal oxidizer formulations, distribution of metal among subpropellants is treated identically to that of binder.

Surface agglomeration of aluminum is calculated using equations developed by Beckstead.[70] Particle ignition delays are calculated as times to heat particles from surface temperature to an assigned ignition temperature (2100 K), while particle burning rates are calculated using an expression by Belyaev.[71] The transpiration gas velocity profile is calculated assuming a linear temperature profile from the surface to the end of the diffusion flame. A force balance on a particle is then integrated from the surface, utilizing a fitted drag coefficient equation assumed (based on Marshall's study[72]) to increase by a factor of 2.5 after ignition, to yield a particle time-distance history. Coupling of this analysis with ignition time and burning rate expressions permits calculation of metal combustion heat release distribution for each metal particle size (agglomerated and unagglomerated) and, finally, calculation (by superposition procedures) of the rate of conductive feedback. Radiative feedback was approximated using a cloud emissivity based on fractional area subtended by particles within an assigned distance from the surface. (For the one metallized formulation tested, radiative transfer had negligible effect on predicted burning rate.) Further details of the treatment of the effects of aluminum on composite propellant combustion are given in Ref. 32.

Two postulated erosive burning mechanisms were utilized. The first, enhancement of transport properties by crossflow-induced turbulence, decreases oxidizer/fuel gas mixing distance and increases effective thermal conductivity between the heat release zones and the surface. In addition, as discussed earlier, columnar diffusion flame bending is postulated to decrease the mixing distance component normal to the surface through distortion of the mixing cone. [It is important to note that detailed examination of outputs from the model indicate that the first mechanism (turbulence-enhanced transport properties) is predicted to have much stronger influence than the second (flame-bending) mechanism in leading to crossflow-induced augmentation of the burning rate.]

Calculation of crossflow effects on burning rate by way of these mechanisms requires a fluid flow analysis for determination of velocity and turbulence profiles. A summary of the procedures follows (details appear in Ref. 54).

First, estimates of burning rate and flame height are made. A nonblowing skin friction coefficient is calculated from empirical flat-plate equations as a function of crossflow Reynolds number and roughness height. It should be noted in passing that there are typographical errors in the equations presented in Ref. 54. Equation (29) in that reference should read

$$C_{f0} = 0.00140 + 0.125Re^{-0.32} \tag{24}$$

and Eq. (30) in that reference should read

$$C_{f0} = 0.95[4 \log_{10}(R/k) + 3.48]^{-2} \tag{25}$$

A blowing parameter b

$$b = 2m_p/(\rho U C_{f0}) \tag{26}$$

U = mainstream crossflow velocity
C_{f0} = nonblowing skin friction coefficient

is then calculated for determination of the actual C_f. Due to a lack of data, particularly at high blowing numbers of interest, several optional expressions relating C_f/C_{f0} to b were initially considered. An expression, based on the work of Kutataladze and Leont'ev,[14] which agreed well with limited data and gave reasonable results on extrapolation was finally selected:

$$C_f/C_{f0} = (1 - b/10)^2/(1 + b/10)^{0.4} \tag{27}$$

As may be noted, this expression yields negative skin friction values for $b > 10$: this is interpreted as indicating boundary-layer separation. For such cases, it is assumed that the velocity profile assumes the cosine shape measured by Yamada and Goto.[12]

With C_f, wall shear stress is calculated in a straightforward manner and substituted into an expression (based on momentum integral analysis) for local shear stress:

$$\tau = \tau_{\mathrm{wall}} + \dot{m}_p u - Ky \tag{28}$$

y = distance from propellant surface
u = local crossflow velocity
K = constant, function of mainstream crossflow velocity, burning rate, and channel dimensions

An eddy viscosity approach is used to relate τ to the local crossflow velocity gradient:

$$\tau = (\mu + \rho\varepsilon)\frac{du}{dy} \quad (29)$$

With specification of an expression relating ε to y and du/dy (discussed later), assumption of a linear temperature profile, and use of expressions relating density and viscosity to temperature, Eqs. (28) and (29) are then combined and numerically integrated from $u = 0$ at $y = 0$ (surface) to yield $u(y)$, $\rho(y)$, $\mu(y)$, and $\varepsilon(y)$. (Streamline shapes are also calculated, permitting calculation of θ.) The eddy viscosity distribution is then used, assuming Reynolds analogy, to calculate total effective conductivity and diffusivity distributions. Total transport property values averaged over appropriate zones are then calculated and used in mixing and heat feedback equations to calculate revised burn rates and flame distances. This procedure is repeated to convergence. (It should be noted that the averaging procedure has been modified from that used for calculations presented in Ref. 54 to better allow for the fact that the effect of gas-phase heat release on burning rate decreases exponentially with distance from the surface. In addition, effects of flame curvature on the flame bending influence have been added.)

Several eddy viscosity models for closure of the boundary-layer analysis were included: All entail use of a Prandtl mixing-length expression

$$\varepsilon = 0.168(y + y_{\Delta})^2(DF)^2\frac{du}{dy} \quad (30)$$

where DF is a damping factor (function of such parameters as blowing ratio, axial pressure gradient, and roughness height), while y_{Δ} is an offset factor dependent on roughness. The most comprehensive form of expression for DF employed was one based on a modified form of an empirical relation developed by Kays and Moffat,[73] which includes the effects of blowing and axial pressure gradient, but does not include the effects of wall (surface) roughness. The modifications added by King were an attempt to include the effects of roughness using approaches suggested by the works of Van Driest[62] and Cebeci and Chang.[63]

As may be seen from Table 2 (presented in Sec. III), there were 10 uncatalyzed HTPB binder composite propellant formulations studied by King in the apparatus depicted in Fig. 4, permitting extensive checkout of the model described above. (Predictions were not made for the catalyzed formulation since the model does not include the capability of treating catalysts; however, the data are included in the following discussion of the effects of various parameters on sensitivity of formulations to crossflow.) The polyester formulations were also not checked against the model since the limited data base for these formulations is inadequate for evaluation of the three "free" constants in the model, which would almost certainly be different for different binder systems. (Recall, the values of the constants for the HTPB-AP formulations were chosen using zero crossflow data for formulations 4525, 5051, 4685, and 5542, the four unimodal oxidizer formulations in the series examined.)

Erosive burning test results are presented in Figs. 8–18, in the form of burning rate vs pressure at various crossflow velocities. In addition, theoretical predictions are presented for all but the catalyzed formulation (4869) in these figures. As may be seen, the agreement between data and predictions for the no crossflow conditions is excellent for all formulations except 7996, where the theoretically predicted burning rates are 10–20% high. In addition, the crossflow effect predictions agree reasonably well with the data in general. With the baseline formulation (4525), the theory slightly underpredicts the effect of crossflow on burning rate, while with 5051, 4685, and 5542 (the other three noncatalyzed unimodal oxidizer

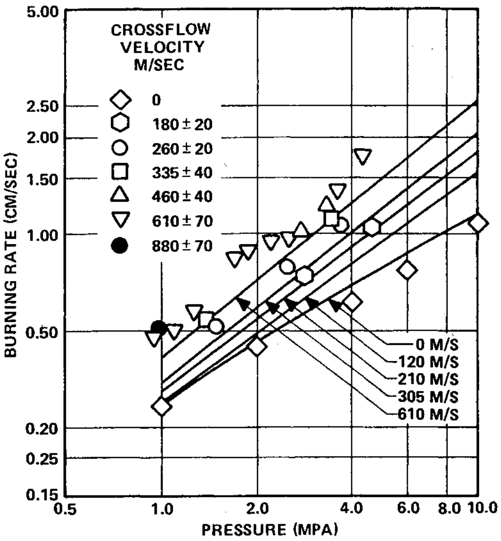

Fig. 8 Burning rate predictions (solid lines) and data (points) for Formulation 4525 (73/27 AP/HTPB, 20-μ AP).

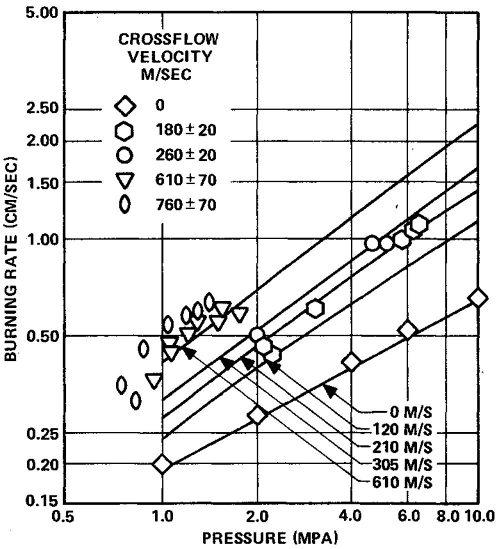

Fig. 9 Burning rate predictions (solid lines) and data (points) for Formulation 5051 (73/27 AP/HTPB, 200-μ AP).

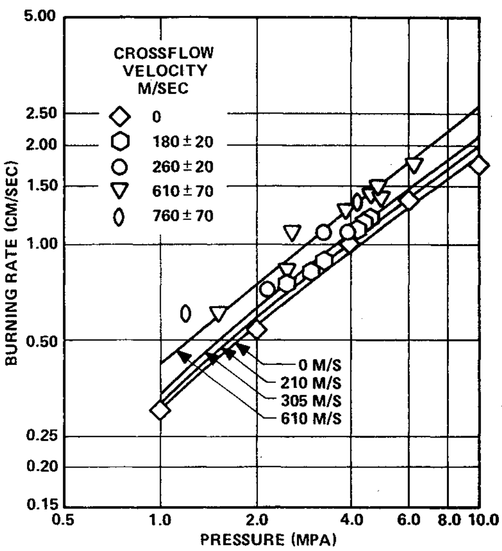

Fig. 10 Burning rate predictions (solid lines) and data (points) for Formulation 4685 (73/27 AP/HTPB, 5-μ AP).

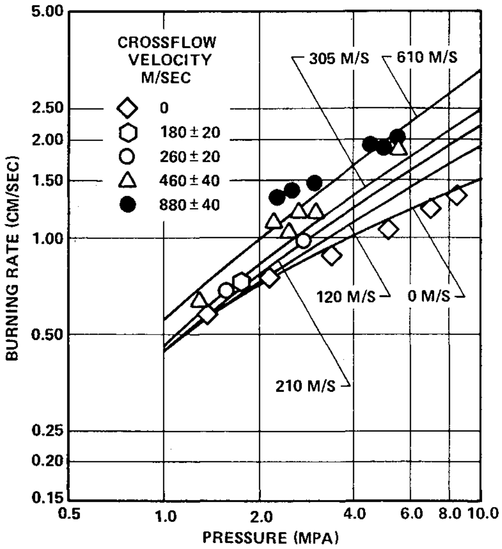

Fig. 11 Burning rate predictions (solid lines) and data (points) for Formulation 5542 (77/23 AP/HTPB, 20-μ AP).

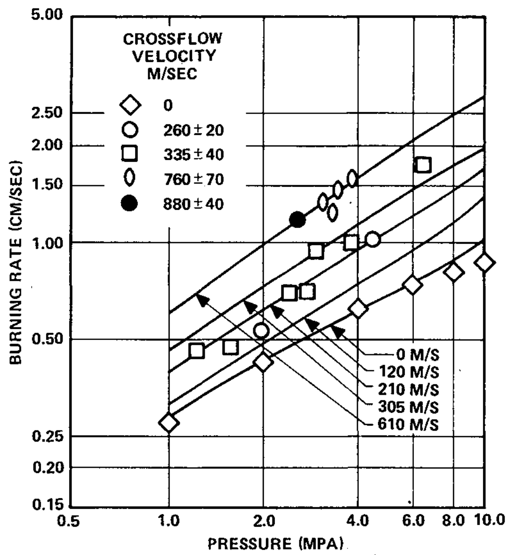

Fig. 12 Burning rate predictions (solid lines) and data (points) for Formulation 5565 (82/18 AP/HTPB, 13.65% 90-μ AP, 68.35% 200-μ AP).

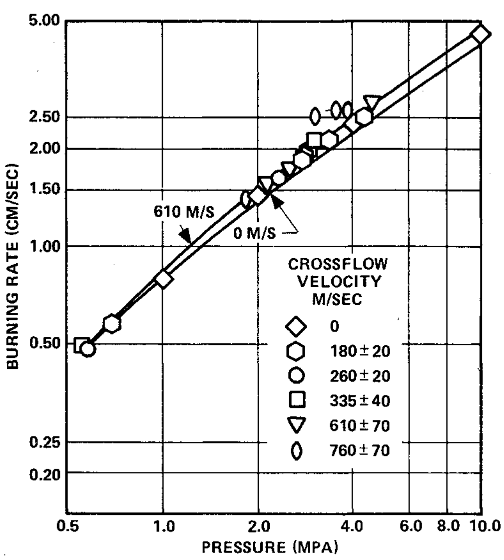

Fig. 13 Burning rate predictions (solid lines) and data (points) for Formulation 5555 (82/18 AP/HTPB, 41% 1-μ AP, 41% 7-μ AP).

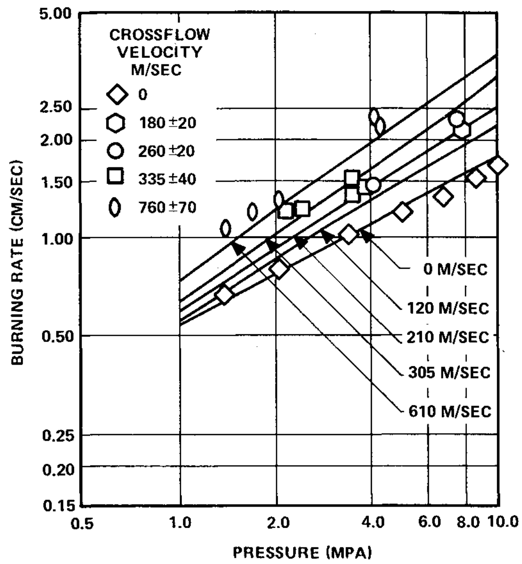

Fig. 14 Burning rate predictions (solid lines) and data (points) for Formulation 7993 (82/18 AP/HTPB, 41% 7-μ AP, 41% 90-μ AP).

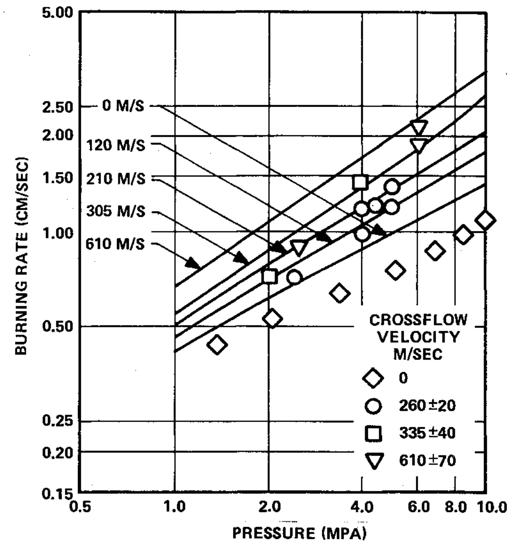

Fig. 15 Burning rate predictions (solid lines) and data (points) for Formulation 7996 (82/18 AP/HTPB, 41% 20-μ AP, 41% 200-μ AP).

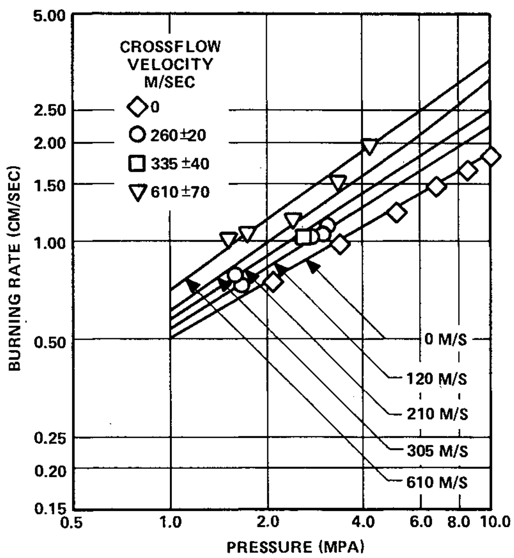

Fig. 16 Burning rate predictions (solid lines) and data (points) for Formulation 8019 (82/18 AP/HTPB, 27.3% 1-μ AP, 27.3% 20-μ AP, 27.4% 200-μ AP).

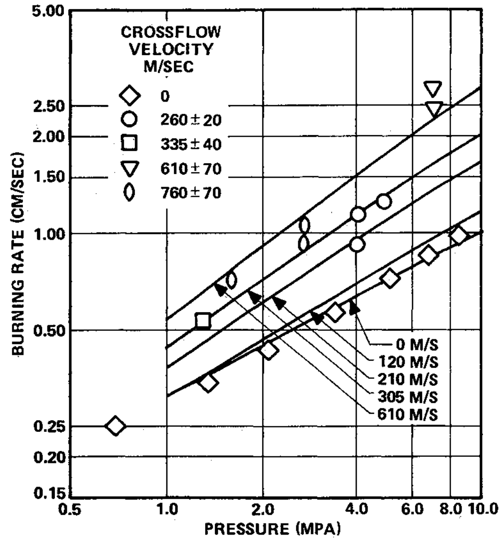

Fig. 17 Burning rate predictions (solid lines) and data (points) for Formulation 6626 (74/21/5 AP/HTPB/Al, 70% 90-μ AP, 4% 200-μ AP).

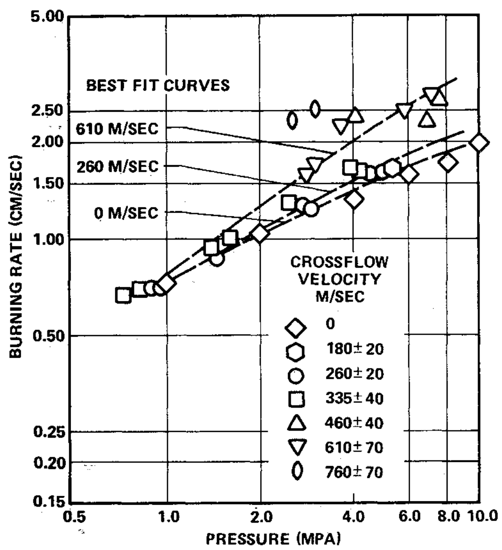

Fig. 18 Burning rate data (no predictions) for formulation 4869 (72/26/2 AP/HTPB/iron oxide, 20-μ AP).

formulations), agreement between theory and data is excellent. The model predicts that the high burning rate formulation (5555) should be quite insensitive to crossflow velocity, in excellent agreement with experiment. Formulation 5565, on the other hand, appears to be slightly less sensitive to crossflow than predicted, particularly at the lower pressures (1–3 MPa). Agreement between theory and data for the remaining three multimodal oxidizer, nonmetallized formulations is good, except that the zero-crossflow offset between theory and data for 7996 appears to be maintained for the crossflow cases. Finally, the rather limited data for the metallized formulation (6626) appear to be in general agreement with predictions.

Results for the various formulations may be compared to identify parameters dominating the sensitivity of burning rate to crossflow. Formulations 4525, 5051, and 4685 were identical except for oxidizer particle size (and, as a consequence) base (no crossflow) burning rate. Examination of Figs. 8–10 reveals that the crossflow sensitivity increases with increasing particle size (decreasing base burning rate). For example, at 200 m/s and 5 MPa, the augmentation ratios for 4685, 4525, and 5051 are about 1.10, 1.60, and 2.00, respectively.

Comparison of data for 4525 and 4869, differing only in use of catalyst in the latter (with consequent higher base burning rate) again shows an increase in crossflow sensitivity with decreasing base rate. At 5 MPa and 200 m/s, their respective burning rate augmentation ratios are 1.60 and 1.10, while at 600 m/s, the r/r_0 values are 2.3 and 1.7. Thus, base burning rate is seen to affect erosion sensitivity even at constant oxidizer size.

Formulations 4685 and 4869 have approximately the same base burning rate at 8 MPa, although their oxidizer sizes are different. Data comparison indicates that these formulations have nearly the same sensitivity to low crossflow velocities at 8 MPa, with the catalyzed propellant being only slightly more sensitive at higher velocities. Thus, it appears that it is the base burning rate rather than the oxidizer particle size which dominates the sensitivity of this series of four 73/27 AP/HTPB formulations to crossflow, though oxidizer size itself does appear to have a slight additional effect, crossflow sensitivity decreasing with decreasing size at constant base rate.

Formulation 5542 differs from 4525 in oxidizer/fuel ratio, and consequently, flame temperature. Since oxidizer particle size was held constant, the higher O/F ratio results in higher base rate for 5542. The data (Figs. 8 and 11) indicate that the crossflow sensitivity of 5542 is considerably lower over the entire range of conditions studied. Comparison of results for 5565 and 4525, which differ in O/F ratio, but have the same base burning behavior (due to compensating AP particle size differences), indicates that the sensitivity of these two formulations to crossflow is nearly identical. Accordingly, it may be concluded that O/F ratio (and consequently, flame temperature) changes do not directly effect the erosion sensitivity of these formulations, but only affect it through their effect on base burning rate.

Formulation 6626 (metallized) has nearly the same base burning characteristics as 4525 and 5565, and approximately the same flame temperature as 5565. The data of Figs. 8, 12, and 17 reveal that all three formulations have quite similar erosive burning characteristics. For example, at 760 m/s and 2.8 MPa, the augmentation ratios for 4525, 5565, and 6626 are 2.1, 2.25, and 2.1, while at 260 m/s and 4.0 MPa, they are 1.65, 1.55, and 1.60. These results support a conclusion that the dominant factor affecting crossflow sensitivity of composite propellants is base burning rate, largely independent of the factors determining that base rate.

Formulations 5555, 5565, 7993, 7996, and 8019 are identical in composition (82/18 AP/HTPB), differing only in oxidizer particle size blends, which were adjusted to give a range of base (zero-crossflow) burning rate vs pressure characteristics. In Fig. 19, data extracted from Figs. 12–16 are plotted in the form of burning rate augmentation factor (r/r_0) vs base burning rate for three combinations of pressure and crossflow velocity. As may be seen, the augmentation factor decreases monotonically and fairly smoothly with increasing base burning rate, again indicating the importance of that parameter on crossflow sensitivity.

A summary of the above comparisons, delineating the effects of various parameters on crossflow sensitivity of burning rate was presented earlier as Table 3. As may be seen from Figs. 8–18, the second generation composite propellant model by King predicts these observed tendencies quite well.

3. *Double-Base Propellant Model*

In the modeling of erosive burning of double-base propellants by King,[55,56] effects of crossflow on a multiple heat release zone combustion wave, as described by Rice and Ginell,[74] were examined. The proposed flame structure (Fig. 20) consists of three separate reaction zones. Heat feedback raises the propellant from its bulk temperature to a temperature, near the surface, at which reaction to preliminary intermediates (gas and/or spray) takes place. These fragments are further heated by the thermal wave until a second set of reactions occurs in a fizz reaction zone. Finally, there is a

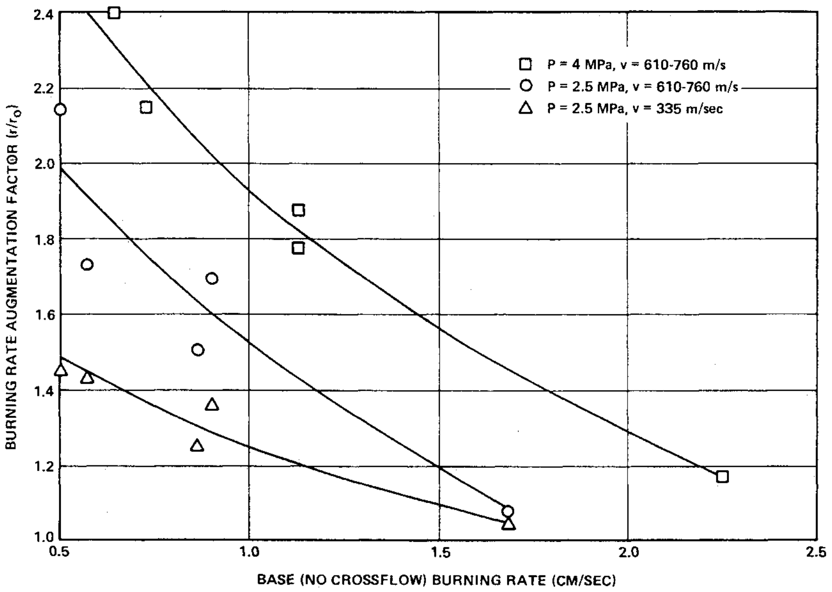

Fig. 19 Summary of results for 82/18 AP/HTPB formulations.

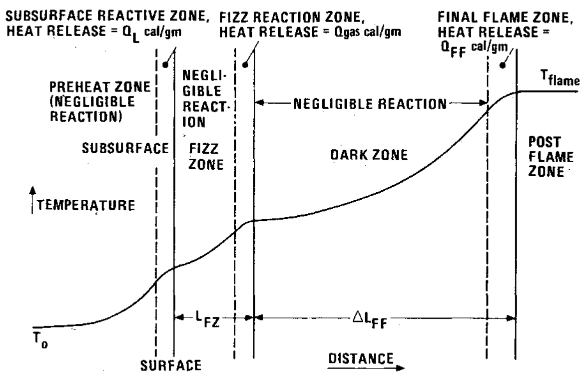

Fig. 20 Postulated double-base propellant flame structure.

long induction zone (dark zone), terminated by a final thin luminous flame zone (reasonably approximated as a flame sheet). In the absence of crossflow, the extreme length of the dark zone and the low molecular conductivity result in negligible heat feedback from the final flame, decoupling it from the burn rate-controlling fizz zone and surface reaction zone processes. However, with crossflow, induced turbulence can increase the average effective thermal conductivity across the dark zone by one to two orders of magnitude, resulting in appreciable heat flux back to the fizz zone and raising its temperature markedly. This, in turn, accelerates reactions in this zone, causing increased heat feedback to the surface.

Crossflow may also accelerate double-base propellant burning rate by penetration of crossflow-induced turbulence into the fizz zone, increasing heat feedback from the fizz reaction zone to the surface. However, due to the gas/liquid froth structure of this zone, it is not clear how effectively such turbulence will penetrate through it. Accordingly, two limiting-case analyses were developed: 1) no turbulence penetration into the fizz zone, with the outer edge of this zone being considered to be an effective surface; and 2) treatment of the fizz zone as a gas, with boundary-layer analysis beginning at the actual propellant surface. (As will be discussed later, only the second model variant gave predictions in good agreement with data.)

First, a model was developed for prediction of burning rate as a function of pressure and heat of explosion in the absence of crossflow. As indicated earlier, under zero-crossflow conditions, the final flame is decoupled and the temperature gradient at the inner edge of the dark zone is zero. The fizz reaction zone is assumed to be infinitesimally thin, its distance from the surface being the product of gas outflow velocity and a characteristic reaction time. Following Beckstead,[75] mass flux and surface temperature are related by

$$\dot{m} = 5000 \exp(-10{,}000/RT_s) \text{ g/cm}^2\text{s} \tag{31}$$

Solution of the Fourier equation (zero source term) between $x = 0$ and $x = L_{fz}$, application of an energy balance at $x = L_{fz}$, with the temperature gradient at the inner side of the dark zone being zero, and application of an overall energy balance (with no feedback from the final flame) yields

$$T_s = T_{dz} - [(T_{dz} - T_s) + c_{ps}(T_s - T_0)/c_{pfz} - Q_L/c_{pfz}] \times [1 - \exp(-\dot{m}c_p L_{fz}/\lambda)] \tag{32}$$

where T_{dz} is the dark zone temperature, Q_L is the net surface/subsurface heat release, and T_0 is the bulk propellant temperature.

Data of Aoki and Kubota[76] relating T_{dz} to P and heat of explosion H_{ex}, may be expressed as

$$T_{dz} = a(P) + bH_{ex} \tag{33}$$

where $b = 0.425$ Kg/cal and $a = 720 + 125\ \ell n(P)$, for $P < 20$ atm and $a = 855 + 80\ \ell n(P)$ for $P > 20$ atm. An empirical expression for Q_L, based on a modification of Beckstead's expression to better allow for observed burning rate trends at low pressure, was also utilized (P in atm):

$$Q_L \text{ (cal/g)} = (65.7 + 0.013H_{ex})(P/6)^{0.08} \tag{34}$$

Finally, L_{fz} was calculated as the product of average gas velocity across the fizz zone and a characteristic reaction time:

$$L_{fz} = \dot{m}RK_{fzrx}(T_{dz} + T_s)\exp(E_{fz}/RT_{dz})/[2P^{\nu}(MW)T_{dz}] \tag{35}$$

From Aoki and Kubota[76] and Beckstead,[75] E_{fz} was set equal to 40,000, and the reaction order ν was chosen to be unity. The reaction rate constant K_{fzrx} was determined by fitting one data point from an extensive burning rate vs pressure and heat of explosion data base generated by Miller.[77]

Substitution of Eqs. (33) and (34) into Eqs. (32) and (35) results in three equations [(31), (32), and (35)] in three unknowns ($\dot{m}$, L_{fz}, and T_s), which are simply solved to give burning rate as a function of pressure and heat of explosion in the absence of crossflow.

The mechanism by which crossflow is assumed to alter burning rate is by augmentation of the thermal conductivity from the surface of the propellant all the way through the final flame zone. The procedure used for calculation of the variation of this parameter with distance from the surface was the same as that described earlier for the second generation composite-propellant erosive-burning model of King. Details of the equation development and solution procedures for both scenarios mentioned earlier, regarding alteration of the fizz zone transport properties by turbulence, are presented in Refs. 55 and 56.

Miller[77] has generated a systematic data base for burning rates of nitrocellulose (12.6 N)/nitroglycerine/secondary plasticizer formulations as a function of pressure and heat of explosion. One of his data points (P = 35 atm, H_{ex} = 950 cal/g) was used to calculate K_{fzrx}, the rate constant appearing in Eq. (35), after which the no-crossflow model was used to predict mass burning fluxes at other pressures and H_{ex} values in his data base. Predicted and measured values are presented in Fig. 21; as may be seen, excellent agreement is observed between the data and predictions.

In Fig. 22, predictions made with the zero-crossflow version of this model are compared with data obtained by Aoki and Kubota[76] for two formulations with much higher NC/NG ratios than those tested by Miller. Agreement between data and predictions is again excellent, at least down to burning mass fluxes of 0.3 g/cm² s, at which point predicted rates begin to exceed measured ones, probably due to the fact that condensed-phase reactions (less well understood) begin to dominate at these low mass fluxes and pressures.

The two erosive-burning model variants (with and without turbulence penetration into the fizz zone) have been tested against data obtained for two NG/NC propellants studied by Burick and Osborn.[78] These formulations, designated as BUU and BDI, have heats of explosion of approximately 1050 and 920 cal/g, respectively. Predicted and observed burning mass fluxes are presented in Figs. 23–26. As may be seen from Fig. 23, the no-crossflow predictions of burning rate vs pressure for BUU are excellent. In addition, the erosive burning predictions made, assuming full turbulence penetration through the fizz zone, are quite good; while the rigid structure fizz zone model results in drastic underprediction of crossflow effects. This is more clearly shown in Fig. 24, where the burning mass flux (predicted and observed) is plotted against crossflow velocity at constant pressure. Effects of crossflow predicted assuming turbulent boundary-layer development starting at the interface of the unburned propellant and the fizz zone agree quite well with data, while the alternate model fails badly. Similar results for the BDI formulation appear in Figs. 25 and 26.

In conclusion, a flame-sheet model of homogeneous double-base propellant combustion for prediction of burning rate as a function of pressure and heat of explosion in the absence of crossflow, has been developed and found to yield excellent agreement between predicted and measured values. Two extensions of this model to treat crossflow have been developed, one allowing for turbulence effects in both the fizz and dark zones, the other allowing such effects only in the dark zone. The former model variant yields predictions in excellent agreement with measured data over a wide range of crossflow velocities.

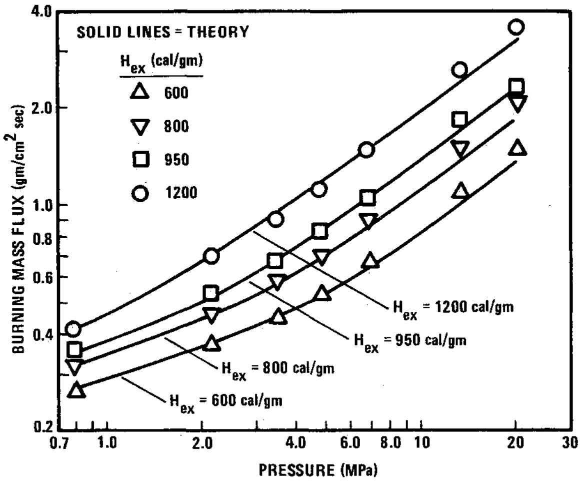

Fig. 21 Comparison of predicted burning rates using a flamesheet model with data of Miller.[75]

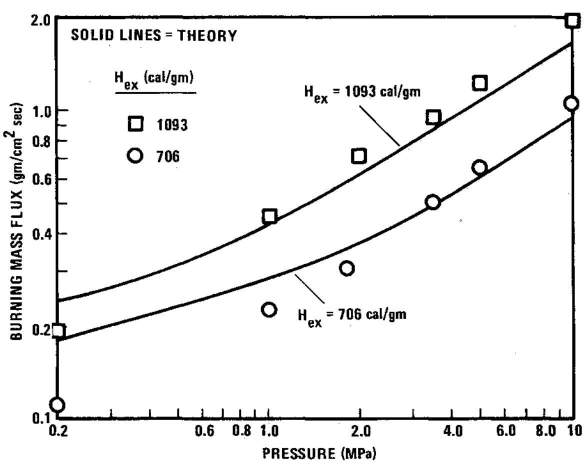

Fig. 22 Comparison of predicted burning rates using a flamesheet model with data of Aoki and Kubota.[74]

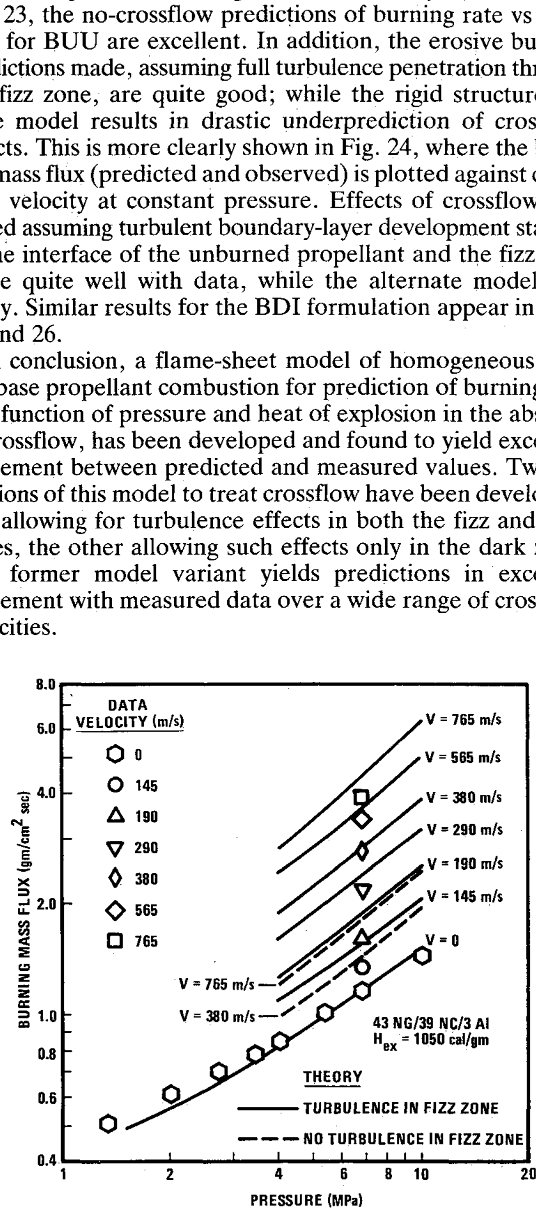

Fig. 23 Predicted and observed burning mass fluxes for BUU propellant.

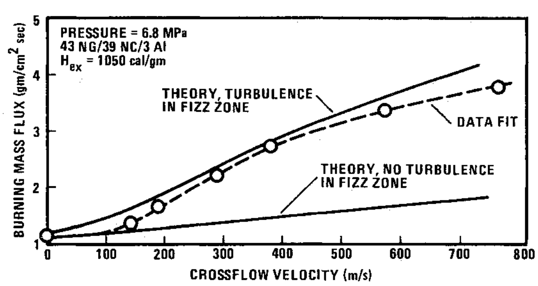

Fig. 24 Predicted and observed effects of crossflow velocity on burning rate of BUU propellant.

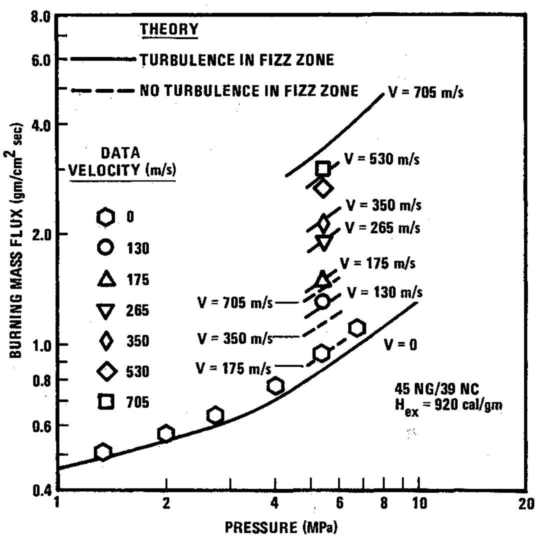

Fig. 25 Predicted and observed burning mass fluxes for BDI propellant.

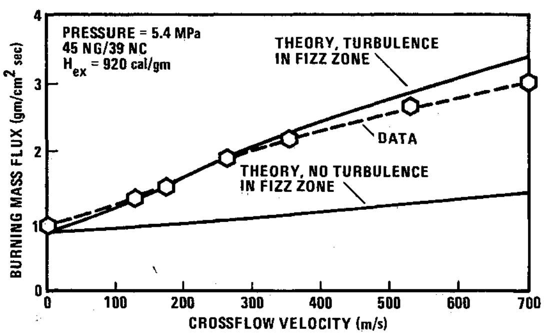

Fig. 26 Predicted and observed effects of crossflow velocity on burning rate of BDI propellant.

VI. Correlations Based on Predicted Results of Complex Models

The comparatively long computer run times associated with exercise of the more complex models described above generally preclude their direct incorporation in solid rocket motor interior ballistics analyses, where they would have to be called on thousands of times to calculate burning rates at each spatial node at each time increment utilized in such analyses. Accordingly, both Arora et al.[79] and King[80] have used their models to develop correlation procedures for much simpler calculations of burning rate as a function of numerous parameters. (King's procedure has been incorporated in a code for analysis of nozzleless rocket motors, as indicated in Ref. 80.) These correlations are described briefly below.

The correlating expression developed by Arora et al.[79] for erosive burning of composite propellants, may be expressed as (using slightly different nomenclature)

$$r_b/r_b^0 = (1 + f_{\mathrm{MP}} f_{\mathrm{Rh}} f_{\mathrm{PG}} f_D)\exp[(\sigma_p - \sigma_p^0)(T_{\mathrm{pi}} - T_{\mathrm{pi},r})] \tag{36}$$

where

$$f_{\mathrm{Rh}} = 1.0 + 0.50\tanh[0.063(MP)^{0.59}R_h - 1]$$
$$= 1.0 \text{ if bracketed term is less than zero} \tag{37}$$

$$f_{\mathrm{PG}} = 1.0 - 0.019\frac{\partial P}{\partial X} \tag{38}$$

$$f_D = 1.0 + 0.1\exp(-2.8D) \tag{39}$$

$$f_{\mathrm{MP}} = 0.40[(M - M_{\mathrm{th}})P]^{0.64}/(aP^n) \quad \text{for} \quad M > M_{\mathrm{th}}$$
$$= 0.0 \qquad \text{for} \quad M = M_{\mathrm{th}} \tag{40}$$

(In this correlation, the four f of Eqs. (37–40) represent corrections for roughness height, pressure gradient, port diameter, and a combination of crossflow Mach number and pressure, respectively.)

r_b = burning rate at roughness height, conditioning temperature, pressure, crossflow Mach number, axial pressure gradient, and port diameter of interest
r_b^0 = zero-crossflow burning rate at standard (baseline) conditioning temperature
σ_p = burning-rate temperature sensitivity under crossflow conditions
σ_p^0 = strand burning-rate temperature sensitivity
T_{pi} = propellant conditioning temperature
T_{pi}^0 = standard (baseline) propellant conditioning temperature
M = crossflow Mach number
M_{th} = threshold crossflow Mach number
P = pressure
R_h = roughness height
$\partial P/\partial X$ = pressure gradient along grain port
D = port diameter
aP^n = base (zero-crossflow) burning rate at the given pressure

In the development of correlations by King[80] (using predictions of erosive burning made with his second generation model) effects of scaling (port diameter) were first examined. For any given propellant, pressure, and crossflow combination, it was found that the predicted burning rate ratio, r/r_0 (burning rate with crossflow divided by zero-crossflow rate) could be related to port diameter by

$$r/r_0]_D = r/r_0]_{D,\mathrm{reference}} - B\ \ln(D/D_{\mathrm{reference}}) \tag{41}$$

with B correlating as a function of the reference r/r_0 value and an effective flame temperature. [For nonmetallized propellants, this is the actual flame temperature, while for metallized propellants $T_{\mathrm{effective}} = T^* + 10$ (wt % metal), T^* being the flame temperature in the absence of burning of the metal.] In this correlation, the reference diameter was arbitrarily selected as 0.1 ft; for this choice, the correlating procedure led to

$$B = G(T_{\mathrm{effective}}/100)^{1/2} \tag{42}$$

where

$$G = -0.85 + 0.85(r/r_0)]_{D=0.1\mathrm{ft}} \quad \text{for} \quad r/r_0 < 1.2$$
$$= -0.0332 + 0.1694(r/r_0)]_{D=0.1\mathrm{ft}} \quad \text{for} \quad r/r_0 > 1.2 \tag{43}$$

with Eq. (41) becoming (D in feet)

$$r/r_0]_D = r/r_0]_{D=0.1\mathrm{ft}} - B\ \ln(10D) \tag{44}$$

Attention was next turned to development of a correlation for r/r_0 at the 0.1-ft port diameter reference condition as a function of pressure, crossflow velocity, and propellant parameters. A large number of calculations were performed with the full model, covering a wide range of pressures, crossflow velocities, and propellant types. Fortunately, it was found that for any given pressure and crossflow velocity, erosive burning ratio could be correlated almost perfectly with just two propellant parameters, base (zero-crossflow) burning rate, and effective flame temperature (with the effect of the second

Table 5 Values of k_1–k_6 [Eqs. (46) and (47)] at various temperatures

T_{eff}, K	V-range	k_1	k_2	k_3	k_4	k_5	k_6
1667	>2000	86.3	0.929	0.00255	0.457	0.913	−0.0217
	<2000			0.258	−0.151	−0.0894	0.1103
2017	>1500	10.93	0.577	0.100	0.040	0.0124	0.0873
	<1500			0.363	−0.136	−0.267	0.1255
2534	All	2.02	0.279	0.0973	0.100	−0.091	0.089
2974	>700	0.805	0.139	0.0131	0.378	0.345	0.0287
	<700			1.122	−0.30	−0.622	0.176

parameter being much less than that of the first). Careful study revealed that r/r_0 could be fit quite well by

$$r/r_0]_{D=0.1\text{ft}} = A_1/r_0^{A_2} \tag{45}$$

(r_0 in cm/s), where A_2 is a function of crossflow velocity and effective flame temperature, and A_1 is a function of these two parameters and pressure. Closed-form correlations of A_1 and A_2 as functions of P (in atmospheres) and V (in ft/s) were developed for several flame temperatures, where the constants in these expressions, k_1–k_6 are functions of flame temperature (as tabulated in Table 5).

$$A_1 = k_3 V^{k_4} P^{[k_5 + k_6 \ln V]} \tag{46}$$

$$A_2 = 1 - k_1 V^{-k_2} \tag{47}$$

(It should be noted that these expressions were inadvertently reversed and the bracketed term was incorrectly not written as a superscript to P in Ref. 80; the corrections were later noted in an Erratum in *Journal of Spacecraft and Rockets*, Vol. 22, 1985, pp. 394–395.

With Eqs. (41–47), the following procedure is used to calculate burning rate ratio (and thus, total burning rate) for specified pressure, crossflow velocity, channel (port) diameter, and propellant. First, logarithmic interpolation of a base (zero-crossflow) burning rate vs pressure table is used to obtain the base burning rate, r_0. Next, A_1 and A_2 are evaluated for tabular values of flame temperature bracketing the actual value, using Eqs. (46) and (47), and the r/r_0 values for a port diameter of 0.1 ft are calculated for these bracketing values using Eq. (45). Linear interpolation is finally used to obtain the reference diameter r/r_0 value at the actual temperature, and Eqs. (41–44) are then used to obtain r/r_0 for the actual port diameter. If this procedure leads to a calculated r/r_0 value of less than unity, it is assumed that this represents being in a boundary-layer blowoff regime, and the r/r_0 value is defaulted to unity.

VII. Scaling

The detailed models of King, Kuo et al., and Godon et al. (and the correlations based on them), discussed earlier, include capability for prediction of effects of motor scale on erosive burning. Both of the correlation procedures discussed in the previous section can readily be shown to predict a decrease in erosive effects with increasing port diameter. In addition, the second generation model of King, and the correlation procedure based on it, show an increase in threshold velocity (minimum crossflow velocity below which erosive burning effects are not predicted) with increased port diameter as demonstrated in calculation results presented in Ref. 32. Both of these predicted trends are in at least qualitative agreement with observations from motor scaleup studies.

In Ref. 10, Beddini presents an approximate analysis for scaling erosive burning threshold conditions as a function of the base (zero-crossflow) burning rate, and motor size. One goal of this analysis which was met was the prediction of the observed fact that the threshold value of crossflow mass flux increases with increased propellant burning rate and increased motor size (port diameter). In this study, it was concluded that the threshold conditions for erosive burning are related to a critical value of the blowing parameter, b [defined by Eq. (26)]; for values of this parameter above the critical value, the mainstream turbulence does not penetrate (subside) into the near-surface flame regions. (As noted earlier, King refers to this condition of $b > b_{\text{critical}}$ as representing boundary-layer blowoff, and also concludes that erosive burning effects are negligible in this case; thus, the King second generation model yields scaling predictions consistent with those of Beddini.) Details of Beddini's application of this criterion to the determination of threshold crossflow velocity for erosive burning are presented in Ref. 10. His final scaling relationship indicates that the value of the crossflow Reynolds number at the threshold point scales mainly with the surface-transpiration Reynolds number to the 1.25 power; this in turn corresponds to the critical crossflow mass flux being approximately proportional to port diameter to the 0.25 power, and to burning rate to the 1.25 power. Accordingly, this relationship predicts the absence of erosive burning for very large motors (such as space booster solid motors) as observed. (As pointed out by Beddini, none of the large (120-, 156-, 260-in. motors), fired up to the time of his publication, had exhibited any erosive burning, consistent with his predictions.) In addition, the relationship developed by Beddini indicates strongly increasing values of threshold crossflow mass flux with increased zero crossflow propellant burning rate, as predicted and observed in the studies by King and discussed earlier.

Recently, Strand and Cohen[22] have been conducting a series of tests with long segmented motors to measure the transition length threshold conditions (axial location at which deviation from nonerosive burning begins), while systematically varying parameters considered to influence the erosive burning phenomenon. From these experimental studies, they have concluded that the threshold conditions can be correlated in terms of critical crossflow Reynolds number, surface transpiration Reynolds number, and motor local length-to-radius (or diameter) ratio by a linear expression

$$Re_c = K(L/R)Re_s' \tag{48}$$

where Re_c is the critical crossflow Reynolds number

$$Re_c = \rho_g U_{\text{crit}} R_{\text{port}}/\mu_g \tag{49}$$

and Re_s' is a reduced surface transpiration (burning rate) Reynolds number

$$Re_s' = \phi \rho_s r R_{\text{port}}/\mu_s \tag{50}$$

This differs from the Beddini correlation as regards the exponent on the transpiration Reynolds number (1.0 vs 1.25) and, more importantly, inclusion of the length/radius ratio term. As a result, in this correlation, the critical crossflow mass flux for onset of erosive burning is directly proportional to propellant burning rate and to the local length to diameter ratio—thus, the L/R ratio rather than the port radius itself is the critical geometrical scaling parameter, and large motor diameter alone will not serve to avoid the erosive burning regime. The authors claim that this conclusion is corroborated by the fact that erosive burning does indeed occur in the early phases of operation of the very large Space Shuttle SRM.

Accordingly, it appears that at this time there is some controversy regarding motor scale effects on threshold crossflow mass flux required for onset of erosive burning, with Beddini claiming that port diameter is the critical scaling parameter, while Strand and Cohen claim that length-to-diameter ratio is the critical scaling parameter; the first scenario leads to the conclusion that large diameter motors are not susceptible to erosive burning, while the latter scenario contradicts this conclusion. Recent modeling studies by Godon et al.[60,61] mentioned earlier support the conclusions of Beddini (see Fig. 13 of Ref. 61 and the accompanying discussion). Further study to resolve this conflict is of considerable importance with regard to scaling of erosive burning data from small (relatively inexpensive) motor tests to large motors.

Acknowledgment

The original version of this material was first published by the Advisory Group for Aerospace Research and Development, North Atlantic Treaty Organization (AGARD/NATO) in AGARD Lecture Series LS-180 "Combustion of Solid Propellants" in July, 1991.

References

[1]Marklund, T., and Lake, A., "Experimental Investigation of Propellant Erosion," *ARS Journal*, Vol. 3, No. 2, 1960, pp. 173–178.

[2]King, M. K., "Review of Erosive Burning Models," JANNAF Workshop on Erosive Burning/Velocity Coupling, Lancaster, CA, March 7–8, 1977.

[3]Ayris, J., and Petrovic, S., "Erosive Burning in Solid Propellant Rocket Motors," AIAA/SAE/ASME/ASEE 26th Joint Propulsion Conf., Orlando, FL, AIAA Paper 90-2215, July 1990.

[4]Razdan, M. K., and Kuo, K. K., "Erosive Burning of Solid Propellants," *Fundamentals of Solid Propellant Combustion*, edited by K. K. Kuo, and M. Summerfield, Progress in Astronautics and Aeronautics, Vol. 90, AIAA, New York, 1984, pp. 515–598.

[5]Parkinson, R. C., and Penny, P. D., "Boundary-Layer Models of Erosive Burning," AGARD Conf. on Solid Rocket Motor Technology, Paper 10, AGARD CP-259, Oslo, Norway, April 1979.

[6]Parkinson, R. C., "Erosive Burning as a Boundary Layer Phenomenon in Rocket Motors," AIAA/SAE/ASME 16th Joint Propulsion Conf., Hartford, CT, AIAA Paper 80-1208, June 30–July 2, 1980.

[7]Traineau, J.-C., and Kuentzman, P., "Ultrasonic Measurements of Solid Propellant Burning Rates in Nozzleless Rocket Motors," *Journal of Propulsion and Power*, Vol. 2, No. 3, 1986, pp. 213–222.

[8]Beddini, R. A., "Reacting Turbulent Boundary-Layer Approach to Solid Propellant Erosive Burning," *AIAA Journal*, Vol. 16, No. 9, 1978, pp. 898–905.

[9]Beddini, R. A., "Aerothermochemical Analysis of Erosive Burning in a Laboratory Solid-Rocket Motor," *AIAA Journal*, Vol. 18, No. 11, 1980, pp. 1346–1353.

[10]Beddini, R. A., "On the Scaling of Solid Propellant Erosive Burning: The Threshold Condition," *Proceeding of the 15th JANNAF Combustion Meeting*, Newport, RI, CPIA Pub. 297, Vol. II, Feb. 1979, pp. 199–216.

[11]Culick, F. E. C., "Rotational Axisymmetric Mean Flow and Damping of Acoustic Waves in a Solid Propellant Rocket," *AIAA Journal*, Vol. 4, No. 8, 1966, pp. 1462–1464.

[12]Yamada, K., Goto, M., and Ishikawa, N., "Simulative Study on the Erosive Burning of Solid Rocket Motors," *AIAA Journal*, Vol. 14, No. 9, 1976, pp. 1170–1177.

[13]Dunlap, R., Willoughby, P. G., and Hermsen, R. W., "Flowfield in the Combustion Chamber of a Solid Propellant Rocket Motor," *AIAA Journal*, Vol. 12, No. 10, 1974, pp. 1440–1442.

[14]Kutatladze, S. S., and Leont'ev, A. I., *Turbulent Boundary Layers in Compressible Gases*, Academic Press, New York, 1964.

[15]Viles, J. M., "Prediction of Rocket Motor Chamber Pressures Using Measured Erosive-Burning Rates," Rohm and Haas, TR S-275 (Contract DAAH01-70-C 0152) Huntsville, AL, Oct. 1970.

[16]Zucrow, M. J., Osborn, J. R., and Murphy, J. M., "An Experimental Investigation of the Erosive Burning Characteristics of a Nonhomogeneous Solid Propellant," *AIAA Journal*, Vol. 3, No. 3, 1965, pp. 523–525.

[17]Vilyunov, V. N., Dvoryashin, A. A., Margolin, A. D., Ordzhonikidze, S. K., and Pokhil, P. F., "Burning of Ballistite Type H in Sonic Flow," *Fizika Goreniya i Vzryva*, Vol. 8, No. 4, 1972, pp. 501–505.

[18]Saderholm, C. A., "A Characterization of Erosive Burning for Composite H-Series Propellants," AIAA Solid Propellant Rocket Conf., Palo Alto, CA, Jan. 29, 1964.

[19]Green, L., "Erosive Burning of Some Composite Solid Propellants," *Jet Propulsion*, Vol. 24, 1954, pp. 9–15.

[20]Kreidler, J. W., "Erosive Burning: New Experimental Techniques and Methods of Analysis," Solid Propellant Rocket Conf., AIAA Paper 64-155, Palo Alto, CA, Jan. 1964.

[21]Peretz, A., "Investigation of the Erosive Burning of Solid-Propellant Grains with Variable Port Area by Means of Interrupted Burning Experiments," *Israel Journal of Technology*, Vol. 3, 1965, pp. 94–101.

[22]Strand, L., and Cohen, N., "Erosive Burning Threshold Conditions in Solid Rocket Motors," AIAA 25th Joint Propulsion Conf., Monterey, CA, AIAA Paper 89-2528, July 1989.

[23]Strand, L., Nguyen, M. H., and Cohen, N. S., "The Scaling of the Threshold Conditions for Solid Propellant Erosive Burning," AIAA/ASME/SAE/ASEE 24th Joint Propulsion Conf., Boston, MA, AIAA Paper 88-3254, July 1988.

[24]Waesche, W., and O'Brien, W. F., "Evaluation of Techniques for Direct Measurement of Burning Rates in Nozzleless Motors," *Proceedings of the 24th JANNAF Combustion Meeting*, Monterey, CA, CPIA Pub. 476, Vol. I, Oct. 1987, pp. 281–292.

[25]Stokes, B. B., Hessler, R. O., and Caveny, L. H., "Erosive Burning of Nonmetallized Composite Propellants," *Proceedings of the 13th JANNAF Combustion Meeting*, Monterey, CA, CPIA Pub. 281, Vol. II, Sept. 1976, pp. 437–451.

[26]Razdan, M. K., and Kuo, K. K., "Measurements and Model Validation for Composite Propellants Under Crossflow of Gases," *AIAA Journal*, Vol. 18, No. 6, 1980, pp. 669–677.

[27]King, M., "Erosive Burning of Composite Propellants," *Proceedings of the 13th JANNAF Combustion Meeting*, Monterey, CA, CPIA Pub. 281, Vol. II, Sept. 1976, pp. 407–435.

[28]Peretz, A., "Experimental Investigation of the Erosive Burning of Solid Propellant Grains with Variable Port Area," *AIAA Journal*, Vol. 6, No. 5, 1968, pp. 910–912.

[29]Dickinson, L. A., Jackson, F., and Odgers, A. L., "Erosive Burning of Polyurethane Propellants in Rocket Engines," *Eighth Symposium (International) on Combustion*, Williams and Wilkins, Baltimore, MD, 1962, pp. 754–759.

[30]Schultz, R., Green, L., and Penner, S. S., "Studies of the Decomposition Mechanism, Erosive Burning, Sonance and Resonance for Solid Composite Propellants," *Combustion and Propulsion*, 3rd AGARD Colloquium, Pergamon Press, New York, 1958.

[31]King, M. K., "Experimental and Theoretical Study of the Effects of Pressure and Crossflow Velocity on Composite Propellant Burning Rate," *Eighteenth Symposium (International) on Combustion*, Combustion Inst., Pittsburgh, PA, 1981, pp. 207–215.

[32]King, M. K., "Predicted and Measured Effects of Pressure and Crossflow Velocity on Composite Propellant Burning Rate," *Proceedings of the 17th JANNAF Combustion Meeting*, Hampton, VA, CPIA Pub. 329, Vol. I, Nov. 1980, pp. 99–122.

[33]King, M. K., "An Investigation of the Effects of Formulation Parameters on Erosive Burning of Composite Propellants," *Proceedings of the 16th JANNAF Combustion Meeting*, Monterey, CA, CPIA Pub. 308, Vol. II, Dec. 1979, pp. 171–191.

[34]Lenoir, J. M., and Robillard, G., "A Mathematical Method to Predict the Effects of Erosive Burning in Solid Propellant Rockets," *Proceedings of the Sixth Symposium (International) on Combustion*, Reinhold Publishing Corp., New York, 1957, pp. 663–667.

[35]Zucrow, M. J., Osborn, J. R., and Murphy, J. M., "The Erosive Burning of a Nonhomogeneous Solid Propellant," American Inst. of Chemical Engineers Symposium Series No. 52, 1964, pp. 23–29.

[36]Saderholm, C. A., Biddle, R. A., Caveny, L. H., and Summerfield, M., "Combustion Mechanisms of Fuel Rich Propellants in Flow Fields," AIAA/SAE 8th Joint Propulsion Specialist Conf., AIAA Paper 72-1145, New Orleans, LA, Nov. 1972.

[37]Lengelle, G., "Model Describing the Erosive Combustion and Velocity Response of Composite Propellants," *AIAA Journal*, Vol. 13, No. 3, 1975, pp. 315–322.

[38]Corner, J., *Theory of the Interior Ballistics of Guns*, Wiley, New York, 1950.

[39]Vandenkerchove, J., "Erosive Burning of a Colloidal Solid Propellant," *Jet Propulsion*, Vol. 28, 1958, pp. 599–603.

[40]Zeldovich, Y. B., "Theory of Propellant Combustion in a Gas Flow," *Fizika Goreniya i Vzryva*, Vol. 7, No. 4, 1971, pp. 463–476.

[41]Geckler, R. E., et al., "Internal Burning Grains and Related

Components for Solid Propellant Rocket Motors," Aerojet Engineering Corp. Rept. 455, Azusa, CA, June 1950.

[42]Parkinson, R. C., and Penny, P. D., "A Transpired Boundary Layer Model of Erosive Burning," AIAA/SAE 14th Joint Propulsion Conf., Las Vegas, NV, AIAA Paper 78-980, July 1978.

[43]Tsuji, H., "An Aerothermochemical Analysis of Erosive Burning of Solid Propellant," *Proceedings of the Ninth International Symposium on Combustion*, Williams and Wilkins, Baltimore, MD, 1963, pp. 384–393.

[44]Klimov, A. M., "Erosive Burning of Propellants," *Combustion, Explosion and Shock Waves*, Vol. 11, No. 5, 1976, pp. 678–681.

[45]Molnar, O., "Erosive Burning of Propellant Slabs," AIAA/SAE 8th Joint Propulsion Specialist Conf., AIAA Paper 72-1108, New Orleans, LA, Nov. 1972.

[46]Miller, E., "Erosive Burning of Composite Solid Propellants," *Combustion and Flame*, Vol. 10, Dec. 1966, pp. 330–336.

[47]King, M., "A Modification of the Composite Propellant Erosive Burning Model of Lenoir and Robillard," *Combustion and Flame*, Vol. 24, 1975, pp. 365–368.

[48]King, M. K., "Erosive Burning of Composite Solid Propellants: Experimental and Modeling Studies," *Journal of Spacecraft and Rockets*, Vol. 16, No. 3, 1979, pp. 154–162.

[49]Razdan, M. K., and Kuo, K. K., "Erosive Burning Study of Composite Solid Propellants by Turbulent Boundary Layer Approach," *AIAA Journal*, Vol. 17, No. 11, 1979, pp. 1225–1233.

[50]Razdan, M. K., and Kuo, K. K., "Turbulent Flow Analysis of Erosive Burning of Cylindrical Composite Solid Propellants," *AIAA Journal*, Vol. 20, No. 1, 1982, pp. 122–128.

[51]Kamath, H., Arora, R., and Kuo, K. K., "Erosive Burning Measurements and Predictions for a Highly Aluminized Composite Solid Propellant," AIAA/SAE/ASME 18th Joint Propulsion Conf., Cleveland, OH, AIAA Paper 82-1111, June 1982.

[52]Wu, X., Kumar, M., and Kuo, K. K., "A Comprehensive Erosive Burning Model for Double-Base Propellants in Strong Turbulent Shear Flow," *Combustion and Flame*, Vol. 53, 1983, pp. 49–63.

[53]King, M. K., "A Model of Erosive Burning of Composite Propellants," *Journal of Spacecraft and Rockets*, Vol. 15, No. 3, 1978, pp. 139–146.

[54]King, M. K., "A Model of the Effects of Pressure and Crossflow Velocity on Composite Propellant Burning Rate," AIAA/SAE/ASME 15th Joint Propulsion Conf., Las Vegas, NV, AIAA Paper 79-1171, June 18–20, 1979.

[55]King, M. K., "Model for Prediction of Double-Base Propellant Burn Rate Including Crossflow Effects," *AIAA Journal*, Vol. 20, No. 10, 1982, pp. 1432–1439.

[56]King, M. K., "A Burning Rate Model for Double-Base Propellants with and Without Product Crossflow," *Proceedings of the First Specialists Meeting (International) of the Combustion Institute*, Paper 7, Vol. I, Section Francaise du *Combustion Institute*, July 1981, pp. 37–42.

[57]Renie, J. P., Condon, J. A., and Osborn, J. R., "Oxidizer Size Distribution Effects on Propellant Combustion," *AIAA Journal*, Vol. 17, Aug. 1979, pp. 877–883.

[58]Renie, J. P., Barger, M. E., and Osborn, J. R., "Effect of Erosive Burning on Pressure and Temperature Sensitivity," *Proceedings of the 16th JANNAF Combustion Meeting*, CPIA Pub. 308, Vol. II, Sept. 1979, pp. 153–169.

[59]Renie, J. P., and Osborn, J. R., "Erosive Burning," *AIAA Journal*, Vol. 21, No. 12, 1983, pp. 1681–1689.

[60]Godon, J. C., Duterque, J., and Lengelle, G., "Solid Propellant Erosive Burning," *Journal of Propulsion and Power*, Vol. 8, No. 4, 1992, p. 741.

[61]Godon, J. C., Duterque, J., and Lengelle, G., "Erosive Burning in Solid Propellant Motors," AIAA 27th Joint Propulsion Conf., El Segundo, CA, AIAA Paper 91-1865, June 1991.

[62]Van Driest, E. R., "On Turbulent Flow Near a Wall," *Journal of Aeronautical Science*, Vol. 23, Nov. 1956, pp. 1007–1011.

[63]Cebeci, T., and Chang, K. C., "Calculation of Incompressible Rough-Wall Boundary-Layer Flows," *AIAA Journal*, Vol. 16, July 1978, pp. 730–735.

[64]Mickley, H. S., and Davis, R. S., "Momentum Transfer for Flow over a Flat Plate with Blowing," NACA TN 4017, Nov. 1957.

[65]King, M., "Model for Steady State Combustion of Unimodal Composite Solid Propellants," 16th AIAA Aerospace Sciences Mtg., Huntsville, AL, AIAA Paper 78-216, Jan. 1978.

[66]Beckstead, M. W., Derr, R. L., and Price, C. F., "The Combustion of Solid Monopropellants and Composite Propellants," *Proceedings of the Thirteenth Symposium (International) on Combustion*, Combustion Inst., Salt Lake City, UT, 1971, pp. 1047–1056.

[67]Waesche, R. H. W., and Wenograd, J., "Calculation of Solid Propellant Burning Rates from Condensed-Phase Decomposition Kinetics," AIAA Paper 69-145, Jan. 1969.

[68]Burke, S. P., and Schumann, T. E. W., *Industrial and Engineering Chemistry*, Vol. 20, 1928, p. 998.

[69]Glick, R. L., and Condon, J. A., "Statistical Analysis of Polydisperse, Heterogeneous Propellant Combustion: Steady-State," *Proceedings of the 13th JANNAF Combustion Meeting*, Monterey, CA, CPIA Pub. 281, Vol. II, Dec. 1976, pp. 313–343.

[70]Beckstead, M. W., "A Model for Solid Propellant Combustion," *Proceedings of the 14th JANNAF Combustion Meeting*, Colorado Springs, CO, CPIA Pub. 292, Vol. I, Dec. 1977, pp. 281–306.

[71]Belyaev, A. F., Frolov, Yu. V., and Korotkov, A. I., *Fizika Goreniya i Vzryva*, Vol. 4, No. 3, 1968, pp. 323–329.

[72]Marshall, R. L., Pellet, G. L., and Saunders, A. S., "An Experimental Study of the Drag Coefficient of Burning Aluminum Droplets," Air Force Rocket Propulsion Lab. Rept. AFRPL-TR-67-223, Vol. II, Aug. 1967, p. 843.

[73]Kays, W. M., and Moffat, R. J., "The Behavior of Transpired Turbulent Boundary Layers," Thermosciences Div., Dept. of Mechanical Engineering, Stanford Univ., Rept. HMT-20, Stanford, CA, April 1975.

[74]Rice, O. K., and Ginell, R., *Journal of Physical Chemistry*, Vol. 54, 1950, pp. 885–917.

[75]Beckstead, M. W., "A Model for Double Base Propellant Combustion," AIAA/SAE/ASME 16th Joint Propulsion Conf., Hartford, CT, AIAA Paper 80-1164, July 1980.

[76]Aoki, I., and Kubota, N., "Combustion Wave Structures of High and Low Energy Double-Base Propellants," AIAA/SAE/ASME 16th Joint Propulsion Conf., Hartford, CT, AIAA Paper 80-1165, July 1980.

[77]Miller, R. R., and Foster, R. L., personal communication, Hercules/ABL, Cumberland, MD, 1980.

[78]Burick, R. J., and Osborn, J. R., *Proceedings of the 4th ICRPG Combustion Conference*, CPIA Pub. 162, Vol. II, Dec. 1967, pp. 57–69.

[79]Arora, R., Wu, X., White, F. X., and Kuo, K. K., "Erosive Burning of Composite Solid Propellants: Mechanism, Correlation, and Grain Design Applications," *Journal of Spacecraft and Rockets*, Vol. 20, No. 1, 1983, pp. 43–48.

[80]King, M. K., "Prediction of Burning Rates in Nozzleless Rocket Motors," *Journal of Spacecraft and Rockets*, Vol. 22, No. 4, 1985, pp. 394–395; see also AIAA Paper 82-1200, 1982.